We thank the reviewer for providing the thoughtful comments and suggestions. Point-to-point responses to all comments are provided below. Corresponding changes in the manuscript are described in *italics*. The inversion is re-performed in response to comments from reviewer #1. The manuscript has been updated based on the new inversion results with track changes.

Response to Reviewer #1 comments:

Comment 1

This manuscript by Chen et al. used the recently developed multiphase CMAQ adjoint model and IASI satellite total NH_3 column observations to constrain the monthly NEI NH_3 emissions at 36 km spatial resolution in April, July, and October in 2011. A hybrid, two-step optimization scheme was applied. First the NEI inventory was nudged towards the posterior values by a mass-balance approach at a much coarser grid (216 km), and then 4D-Var inversion was performed using the updated inventory as the prior. The posterior emissions were then used to drive the CMAQ model, and the simulated NH_3 abundance, NH_4 deposition, and aerosol chemical composition were evaluated against independent observational datasets. Overall this work is solid, has applied state-of-the art satellite data and CTM tools, and could advance our limited understanding on the emission of NH_3 if its methodology can be fully justified. Hopefully the paper can be further improved after addressing my comments below.

Response

We thank the reviewer for providing insightful comments. In this revision, we addressed these comments carefully. In particular, the inversion was re-performed using daily IASI-NH_3 averages as constrain and revised error terms. The revisions help partly resolved the over-adjustment issue we encountered in Pennsylvania and surrounding regions. Please see our point-by-point responses for details. We hope that this new version of the manuscript has addressed all the concerns raised by the reviewer.

Comment 2

NEI 2011 covers the entire year continuously but this work only focused on three months, April, July, and October. Presumably the computing cost prohibited optimizing NEI for other months, but this should be discussed. Many CTM users would use multiple months or the entire year of NEI, and those three isolated months would hinder further application of the results of this work. Especially, the month of May will be a significant opportunity missed as a large fraction of fertilizer application happens in May, leading to abruptly different emission and column density dynamics relative to April and June.

Response

We thank the reviewer for pointing this out. Yes, we focused on three months because the computational cost to run full year simulation using adjoint model is too high. The CPU time required for one-day forward and adjoint simulation is 9.5 hours and 48 hours, respectively, which means that it takes over 20,000 CPU hours to perform a full year simulation. If the inversion takes 3~5 iterations to reach the converge criteria, the CPU time can reach 60,000 to 100,000 hours. A sentence is added to line 155 to clarify that the optimization only focused on three months due to the high computational cost as follows. "*Limited by the high computational cost of adjoint-model-based inversion, the optimization is only performed for the three months selected instead of a full year.*" In addition, as explained in the sentence in line 155 to 156, the optimization was not performed for the winter months (November, December and January) because the IASI-NH_3 observations are too noisy to serve as a reliable constrain.

The comparison between monthly average IASI NH_3 column density and CMAQ simulated values using the *a priori* NH_3 emission inventory for all twelve months in 2011 are provided in the revised SI (**Figure S9**). Simulated NH_3 column densities are biased low comparing to the IASI observed ones especially from April to August. For May, the simulated NH_3 column densities are much lower than the IASI observations, especially in southern states (Texas and Oklahoma). Although we only performed the inverse modeling in April to represent the spring months, we expect

the emission and column density dynamics in May are similar to those in April. Sentences are added in line 287 to imply the potential low bias of NH_3 emission estimates in the NEI inventory in other months. "*Although the inversion is only applied for the three selected months, the simulated NH_3 column densities using the a priori inventory are consistently lower than the IASI-NH_3 observations in 2011 (**Figure S9**), suggesting that the NH_3 emission estimates in 2011 NEI may be biased low in other months, too.*"

Figure S9 was added to SI to provide the results of the comparison between monthly average IASI NH_3 column density and CMAQ simulated values using the *a priori* NH_3 emission inventory for all twelve months in 2011.

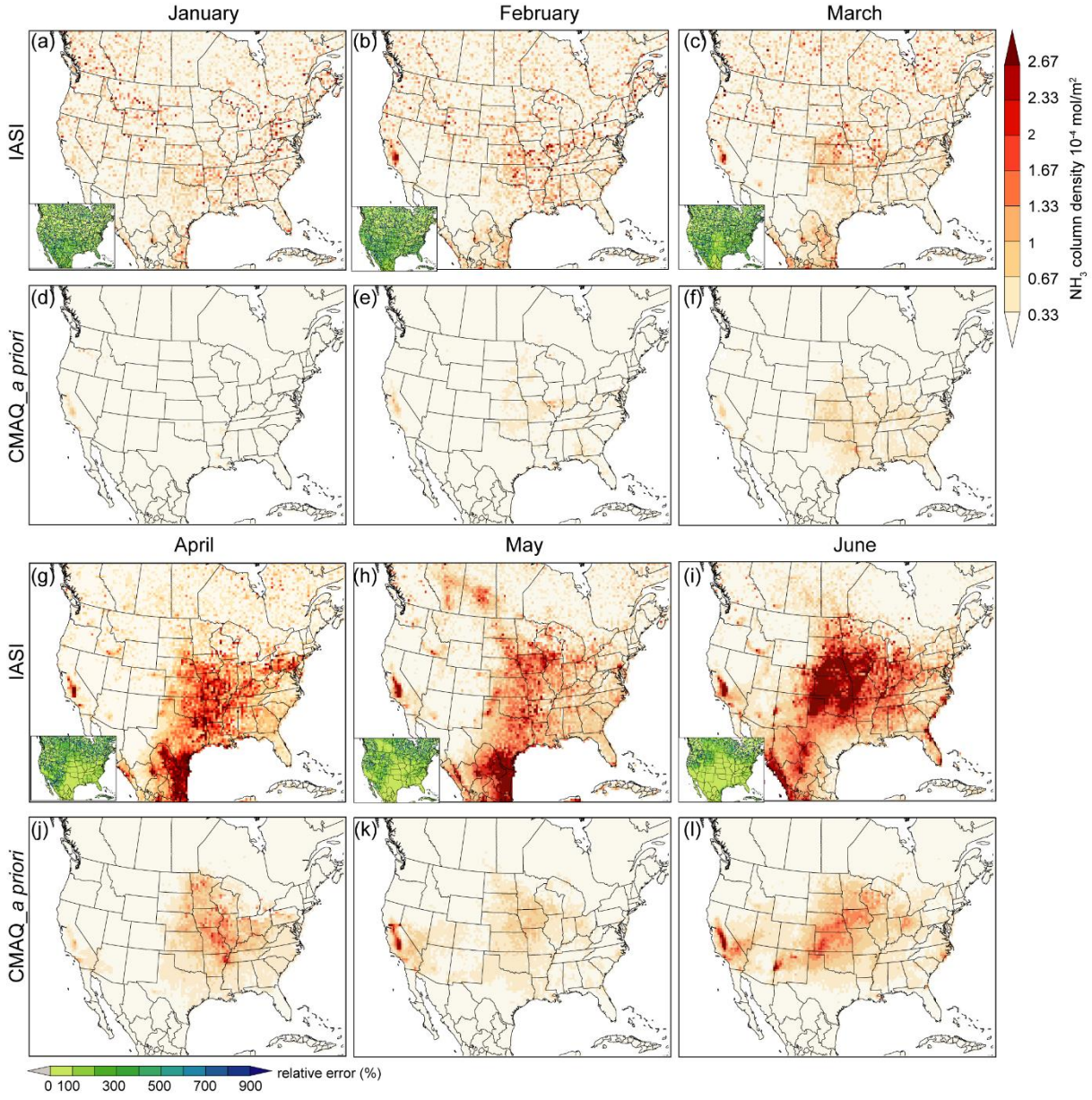

Figure S9 Comparison between monthly average IASI NH_3 column density (a-c, g-i, m-o, s-u) and CMAQ simulated values (d-f, j-l, p-r, v-x) based on the *a priori* NH_3 emission inventory in 2011. The monthly average relative error associated with the observed IASI NH_3 column density is shown in the corner of the corresponding plots.

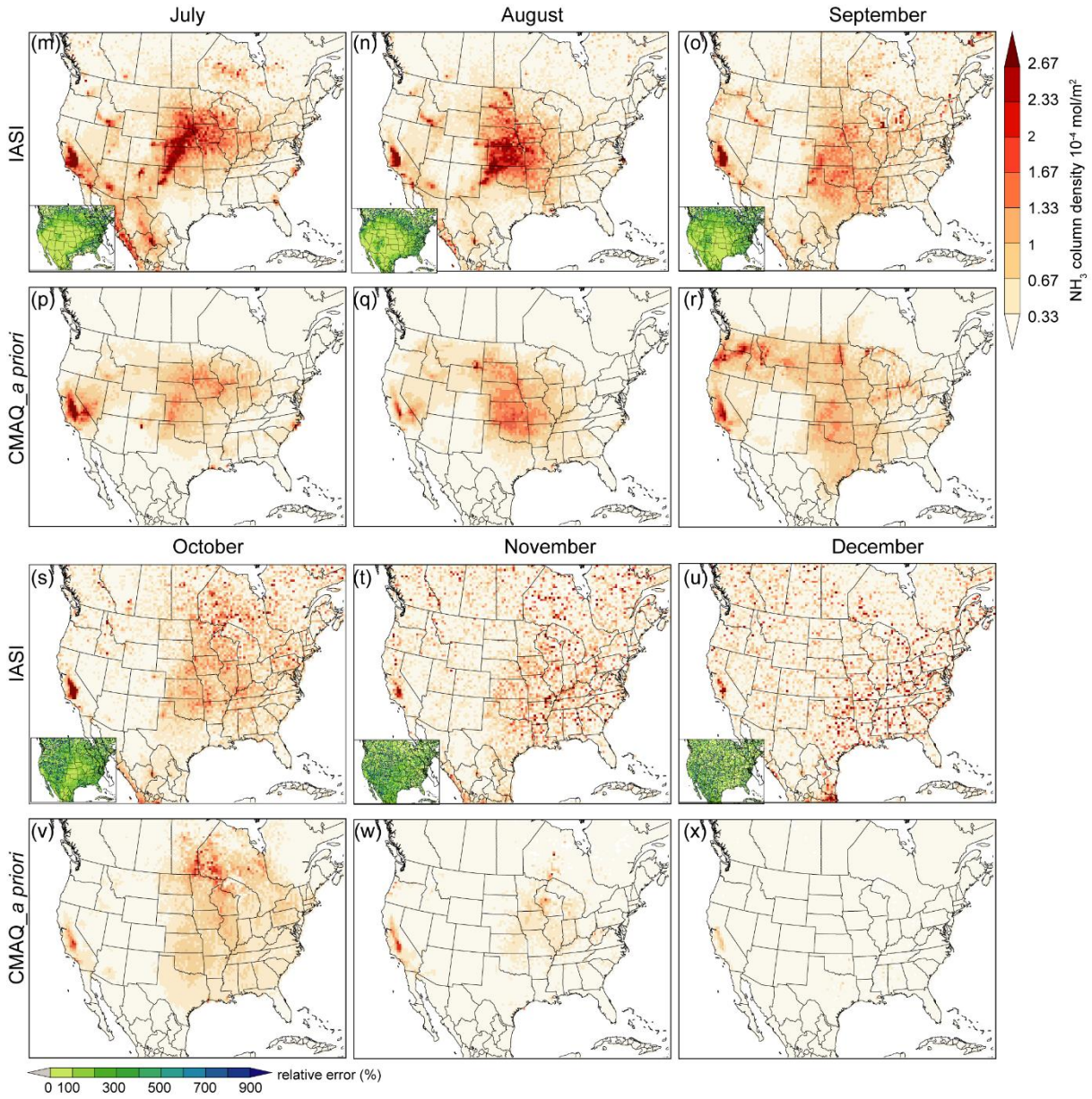

Figure S9 (continued) Comparison between monthly average IASI NH_3 column density (a-c, g-i, m-o, s-u) and CMAQ simulated values (d-f, j-l, p-r, v-x) based on the *a priori* NH_3 emission inventory in 2011. The monthly average relative error associated with the observed IASI NH_3 column density is shown in the corner of the corresponding plots.

Comment 3

The observation used in the inversion seems to be monthly averaged data over 36-km grid cells, and the grid average absolute error was used in the observational error covariance matrix. This may have led to the counterintuitively high values in Pennsylvania and southern Texas, as the monthly averaged grid value could have been driven by a few

anomalously high observation dates, given the sparsity of IASI pixels. The error term (in Equation 1) does not include the scaling of the square root of N (the central limit theorem). As a result, if a grid cell contained only one day with extremely high values (the other days in the month were missing), it would be treated the same way as if all 30 days were those high values. Specifically, the high emissions in Pennsylvania, western New York, and east/south Texas (Fig. 3d) that were seemly driven by high IASI values in April (Fig. 1a) are hard for me to believe. It might be helpful to check IASI April data in other years, e.g., 2010 and 2012, to see if those high column abundance (and consequently high posterior emissions) are consistent.

Response

The reviewer's thought is well-taken. Indeed, using monthly averaged NH_3 column densities and averaged absolute error may lead to biased posterior emission estimates when the high averaged values are driven by high observations in several days. In response to this comment, we redid the inversion using daily observations as constraints. We also change the method to calculate the error term. A simple standard error of the mean column density in each grid was used. Please note that this was achieved by rerunning all the simulations, which was one of the main reasons we postponed the revision due date.

The specifics are described as follows.

The sentence in lines 146-147 is revised as "*The mean column density (Ω_o) is calculated as the arithmetic mean of all retrievals with their centroids falling in the same grid cell, following …*"

The sentence in line 148-153 is revised as "*The error (molec/cm^2) corresponding to the mean column density in each grid is calculated as:*

$$\bar{\sigma} = \sqrt{\frac{\sum(\sigma_i \times \Omega_i)^2}{n-1}}$$

where $\bar{\sigma}$ is the mean error (molec/cm^2), Ω_i is the NH_3 column density from IASI-NH_3 level 2 data, σ_i is the relative error associated with each Ω_i as reported, n is the number of retrievals within each grid cell during the defined time period. For 4D-Var inversion and IMB inversion, daily and monthly means and errors are calculated, respectively."

For the iterative mass balance optimization (IMB) step, the emission scaling factors are still derived at 216 km by 216 km resolution. However, in each day, only grid cells with satellite observations at 36 km by 36 km resolution are adjusted. Otherwise, the grid cells without observations at 36 km by 36 km resolution may be over-adjusted in the IMB step and there will not be enough constraint in the 4D-Var inversion to further adjust the emissions in these grid cells.

The sentences in line 178-185 are revised as "*The first step is to apply the IMB approach to adjust the a priori (2011 NEI) NH_3 emission at 216 km by 216 km resolution (referred to as the coarse grid cell hereafter) based on the ratio between the monthly-averaged observed and simulated NH_3 column density at the satellite overpassing time, iteratively. At each iteration, the emission in each 36 km by 36 km grid cell (referred to as the fine grid hereafter) is scaled by the ratio following the equation below,*

$$E_{t,i,j} = \begin{cases} \frac{\Omega_{o,m}}{\Omega_{a,m}} \times E_{a,i,j}, & IASI\ pixels\ available\ in\ grid\ cell\ i\ in\ day\ j \\ E_{a,i,j}, & no\ IASI\ pixels\ in\ grid\ cell\ i\ in\ day\ j \end{cases} \quad (2)$$

where $E_{t,i,j}$ and $E_{a,i,j}$ are the new and a priori emission estimates in fine grid cell i within the coarse grid cell on the jth day of the month, respectively. $\Omega_{o,m}$ and $\Omega_{a,m}$ are the monthly-averaged observed and simulated NH_3 column density in coarse grid cells, respectively. It is a modified version of IMB optimization performed in previous studies (Li et al., 2019; Cooper et al., 2017; Martin et al., 2003). The emissions in grid cells without IASI retrievals are kept unchanged to avoid over-adjustment."

The sentence in line 190 is revised as "*The final scaling factor (ε_0) for each grid cell is the multiplication of the scaling factors derived at each iteration.*"

For the 4D-Var inversion, daily mean column density from the IASI-NH_3 observations are used as constraints. Daily emission scaling factors are derived through optimization.

The sentences in lines 119-210 are revised as below.

"

$$J = \gamma(\varepsilon - \varepsilon_0)^T S_a^{-1}(\varepsilon - \varepsilon_0) + \left(\Omega_{o,d} - F(\varepsilon)\right)^T S_o^{-1}(\Omega_{o,d} - F(\varepsilon)) \quad (3)$$

*ε is the daily emission scaling factor to be optimized at each iteration where $\varepsilon = log\left({E_t}/{E_a}\right)$ on the 36 km by 36 km CMAQ grid, consisting of 6104 elements overland grid cells in CONUS. $\Omega_{o,d}$ is daily-averaged IASI-NH_3 column densities and F(ε) is CMAQ simulated NH_3 column density sampled at the satellite passing time if there is at least one IASI-NH_3 retrieval in that grid cell. S_a and S_o are error covariance matrices for the a priori emission estimates and IASI-NH_3 retrievals, respectively. The two matrices are assumed to be diagonal. For S_o, the simple standard error corresponding to $\Omega_{o,d}$ is used to represent the observational error (Equation (1)). Our test shows that negative $\Omega_{o,d}$ will lead to a continuous decrease in the adjusted emission for the grid cell because modeled column density cannot become negative. To limit the influence of these negative $\Omega_{o,d}$, their original weights are multiplied by 0.01. For S_a, the uncertainty in each grid cell is assumed to be 100% of the a priori emissions. γ is the regularization factor balancing the relative contribution of the a priori emission inventory and IASI-NH_3 retrievals to the J value. γ is chosen to be 800 for April and 500 for July and October based on the L-curve criteria (Hansen, 1999) (**Figure S5**).*"

Using daily mean IASI-NH_3 column densities as constraints do help alleviate the over-adjustment in Pennsylvania in April. The *posterior* emission estimate in Pennsylvania is 127% higher than the *a priori* estimates using daily means as constraint, whereas 717% higher when using monthly means. For Texas, the difference is smaller (237% higher using daily means versus 335% higher using monthly means) because high IASI-NH_3 column densities were observed on many days, possibly because of the warmer weather condition and earlier fertilizer application activities in 2011. Please refer to the response to **Comment 11** for a detailed discussion. Again, we thank the reviewer for providing this insightful comment on the inversion method.

Comment 4

Page 2, line 49: clarify which NEI it is (prior or posterior) in "NEI-based" assessments.

Response

Thanks for the suggestion. The sentence is revised as "*The model results suggest that the estimated contribution of ammonium nitrate would be biased high in a priori NEI-based assessments.*"

Comment 5

Page 2, lines 61-65: this sentence might fit better at the last paragraph of the introduction.

Response

We thank the reviewer for this suggestion. The sentence in lines 61-65 is moved to the beginning of the last paragraph of the introduction. The last paragraph is revised as "*This work utilizes satellite observations from the IASI NH_3 column density measurements (IASI-NH_3) (Clarisse et al., 2009;Van Damme et al., 2017), to provide a high-resolution, optimized NH_3 emission inventory for the U.S. developed using an adjoint inverse modeling technique (Li et al., 2019), the robustness of which is demonstrated by evaluation against multiple independent in-situ measurements. The IASI-NH_3 dataset was applied to optimize NH_3 emission estimates from the 2011 National Emission Inventory (NEI 2011) using CMAQ and its adjoint model at a 36 km×36 km resolution. …*"

IASI is spelled out at its first appearance in line 70 as "*Several studies have utilized NH_3 column density retrieved from the Infrared Atmospheric Sounding Interferometer (IASI) (Clarisse et al., 2009; Van Damme et al., 2015b) …*"

Comment 6

Page 5, equation 1: this is a strange statistic to calculate. As indicated a few lines above, Ω_0 is the monthly arithmetic mean within a grid cell, but the $\sum(\sigma_i/\sigma_i^2)/\sum(1/\sigma_i^2)$ term is the variance-weighted mean of error. A simple standard error of the mean or standard error of the weighted mean (https://doi.org/10.1016/1352-2310(94)00210-C) might be better choices.

Response

In response to this comment, the error term is changed to a simple standard error of the daily mean in the revised manuscript, and the simulations are re-performed with the revised error covariance matrices. The results are updated throughout the text.

The sentence in line 148-153 is revised as "*The error (molec/cm^2) corresponding to mean column density in each grid cell is calculated as:*

$$\bar{\sigma} = \sqrt{\frac{\sum(\sigma_i \times \Omega_i)^2}{n-1}}$$

where $\bar{\sigma}$ is the mean error (molec/cm^2), Ω_i is the NH_3 column density from IASI-NH_3 level 2 data, σ_i is the relative error associated with each Ω_i as reported, n is the number of retrievals within each grid cell during the defined time period. For 4D-Var inversion and IMB inversion, daily and monthly means and errors are calculated, respectively."

Comment 7

Page 7, lines 201-202: how justified is it to assume that the a priori covariance matrix is diagonal? The error/bias in NEI often seem spatially correlated.

Response

Thank you for raising this concern. The error covariance matrix is assumed to be diagonal because there is no data available to estimate the spatial correlation of errors in NH_3 emission estimates. Including non-diagonal terms to the *a priori* covariance matrix, therefore, may further introduce uncertainties in the inverse modeling. The sentence in line 201-202 is revised to clarify the reason why the *a priori* covariance matrix is assumed to be diagonal as follow. "*With limited information on the spatial correlation of the error covariance, the two matrices are assumed to be diagonal (Paulot et al., 2014; Zhu et al., 2013).*"

References

Paulot, F., Jacob, D.J., Pinder, R.W., Bash, J.O., Travis, K., Henze, D.K.: Ammonia emissions in the United States, European Union, and China derived by high-resolution inversion of ammonium wet deposition data: Interpretation with a new agricultural emissions inventory (MASAGE_NH_3). J. Geophys. Res. Atmos. 119, 4343-4364, https://doi.org/10.1002/2013JD021130, 2014.

Zhu, L., Henze, D. K., Cady-Pereira, K. E., Shephard, M. W., Luo, M., Pinder, R. W., Bash, J. O., and Jeong, G. R.: Constraining U.S. ammonia emissions using TES remote sensing observations and the GEOS-Chem adjoint model, J. Geophys. Res. Atmos., 118, 3355-3368, https://doi.org/10.1002/jgrd.50166, 2013.

Comment 8

Page 7, lines 203: it is important to let the readers understand if the observation vector used in the inversion is composed of single IASI pixels (level 2) or regridded maps (level 3). My impression is that the level 3 regridded IASI

data were used. In that case, the single sounding detection limit of 4.8×10^{15} is not relevant as the averaging will reduce the noise level, and it is important to consider the number of averaging per grid cell.

Response

Yes, level 3 regrided IASI data is used in the inversion. In response to comment 3, the inversion was re-performed and daily means regrided at 36 km 36 km resolution were used as constraints in the 4D-Var inversion. The reviewer is right that the single sounding detection limit is higher than the actual noise level when pixels are averaged. We no longer add a detection limit to the error covariance S_o. The simulations are re-performed with the revised error covariance matrices, and the results are updated throughout the text.

This sentence in lines 203-205, "*To reduce the influence of retrievals close to or below the detection limit, an estimated detection limit of 4.8×10^{15} molecules/cm^2 is added to the S_o (Dammers et al., 2019)*", is deleted.

Comment 9

Page 7, line 215: the convergence criterion that J decreases by less than 2% seems large and arbitrary.

Response

The convergence criterion was chosen following previous inverse modeling studies to optimize NH_3 emission estimates. Citations are added in the sentence in line 215 to clarify the choice of the convergence criterion. "*The iteration process is terminated when the decrease in J is less than 2% or the local minimum is reached (Li et al., 2019; Zhu et al., 2013).*"

References

Li, C., Martin, R. V., Shephard, M. W., Cady-Pereira, K., Cooper, M. J., Kaiser, J., Lee, C. J., Zhang, L., and Henze, D. K.: Assessing the Iterative Finite Difference Mass Balance and 4D-Var Methods to drive ammonia emissions over North America using synthetic observations, J. Geophys. Res. Atmos., 124, 4222-4236, https://doi.org/10.1029/2018jd030183, 2019.

Zhu, L., Henze, D. K., Cady-Pereira, K. E., Shephard, M. W., Luo, M., Pinder, R. W., Bash, J. O., and Jeong, G. R.: Constraining U.S. ammonia emissions using TES remote sensing observations and the GEOS-Chem adjoint model, J. Geophys. Res. Atmos., 118, 3355-3368, https://doi.org/10.1002/jgrd.50166, 2013.

Comment 10

Figure 2: please consider adding the residual map (IASI column-modeled column) as inserts, similar to Fig. 1.

Response

Residual maps are inserted as suggested by the reviewer. Figure 2 is revised as follows,

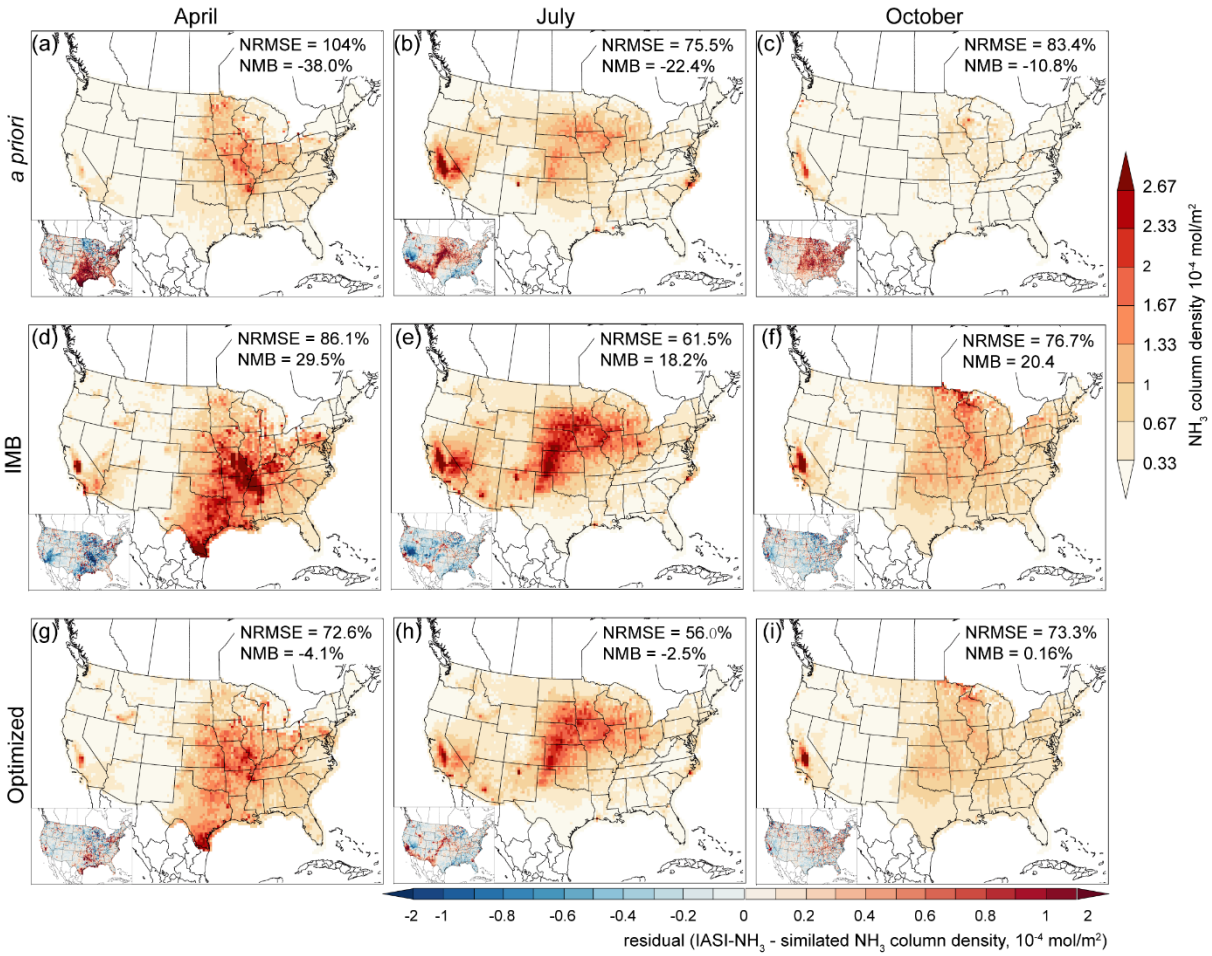

Figure 2 CMAQ simulated monthly average NH_3 column density for April, July, and October 2011 using the *a priori* emissions (a, b, c), the emissions adjusted by IMB (d,e,f), and the final optimized emissions using the hybrid approach (g,h,i). For comparison with the IASI-NH_3 retrievals, simulated NH_3 columns at the passing time are derived when there are observations in that grid cell. Normalized root mean square error (NRMSE) and normalized mean bias (NMB) between the simulated values and IASI-NH_3 are provided. Residue map (IASI-NH_3 – simulated NH_3 column densities) is shown in the corner of each plot.

Comment 11

Page 8, lines 234-235: please define the exact location of NRMSE that reduced by 98%. The high NH_3 observations in April in southern states seem curious and may warrant a closer investigation.

Response

By "southern states" we are referring to the states in the southern region defined by the USDA Farm Production region, which includes Texas and Oklahoma. In the revised simulation, the NRMSE in the southern states was reduced by 50% instead of 98% with the optimized NH_3 emission estimates. The sentence in lines 234-235 is revised as follows "*The optimized NH_3 emission successfully captures the high NH_3 column density in southern states (Texas and Oklahoma), reducing the NRMSE by half in that region.*"

The enhanced NH_3 emissions in the southern states in the optimized emission estimates are more consistent with the total NH_3 emission estimates when air-surface bidirectional exchange is considered (Shen et al., 2020). The ratio between NH_3 emission estimates in southern states and total NH_3 emission within CONUS is 20% and 18% in the optimized estimates and estimates including NH_3 bidirectional exchange in 2011, respectively. In comparison, the ratio is only 10% in the *a priori* NEI estimates.

The comparison of IASI-NH_3 in 2011 and adjacent years shows a substantial variation in the retrieved NH_3 column densities in the southern states. The NH_3 observations are the highest in 2011 and the lowest in 2010 in April and May. The difference coincides with the higher surface temperature in the southern states in these two months. NH_3 volatilization from agricultural lands will increase under warmer conditions (Shen et al., 2020).

The pieces of evidence mentioned above are incorporated in the discussion to support the increased NH_3 emission in southern states in the optimized estimates as follows. The sentences in line 261-263 are revised as "*The higher NH_3 emission estimates in the southern states are driven by the enhanced NH_3 column densities from IASI over that region. IASI-NH_3 column densities are higher in 2011 than those in adjacent years (**Figure S7**), which coincides with the higher surface temperature observed in 2011 (NOAA 2019)(**Figure S8**). NH_3 emission will increase due to enhanced NH_3 volatilization from agricultural lands under warmer conditions (Bash et al., 2013; Shen et al., 2020). In fact, the optimized NH_3 emission pattern in April is more consistent with the spatial pattern of inorganic nitrogen fertilizer estimated based on plant demand (Cooter et al., 2012). NH_3 emission in 2011 estimated by CMAQ with NH_3 bidirectional exchange model also predicted higher NH_3 emission in the southern states (Shen et al., 2020). The ratio between NH_3 emission estimates in southern states and that within CONUS is 26% and 18% in the optimized estimates and estimates including NH_3 bidirectional exchange, respectively. In comparison, the ratio is only 10% in the a priori NEI estimates, suggesting a potential low bias in 2011 NEI.*"

Two figures were added to SI as follows to provide the IASI-NH_3 column densities for 2010, 2011, and 2012 and surface temperature maps for these three years.

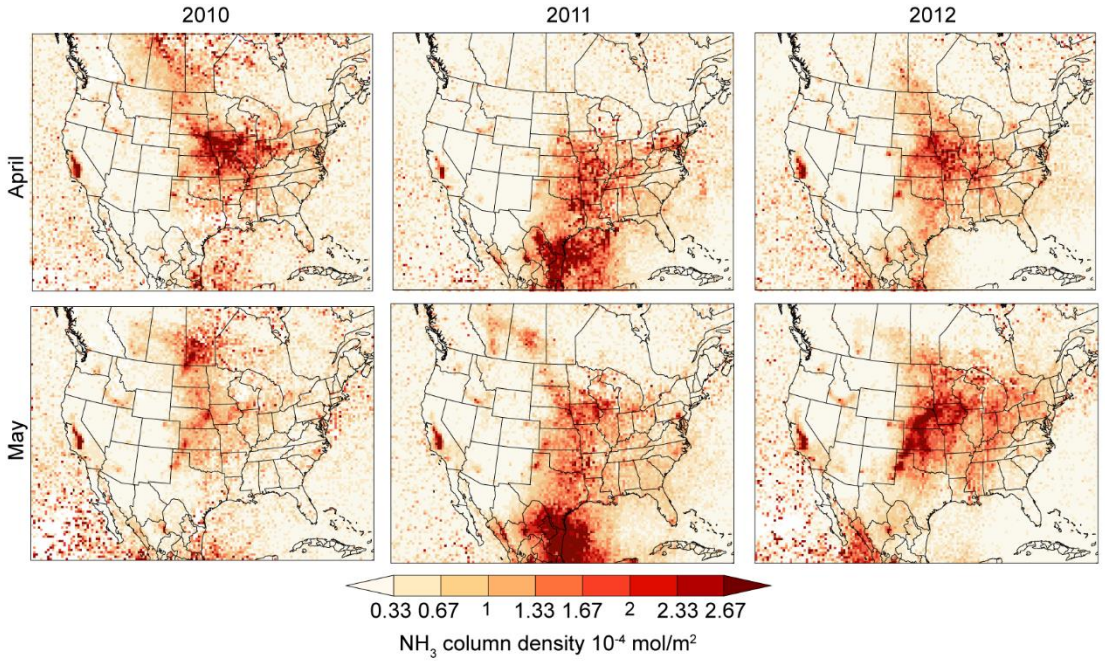

Figure S7 Monthly averaged IASI-NH3 column densities in April and May from 2010 to 2012. The satellite retrievals are regridded at 36 km by 36 km resolution.

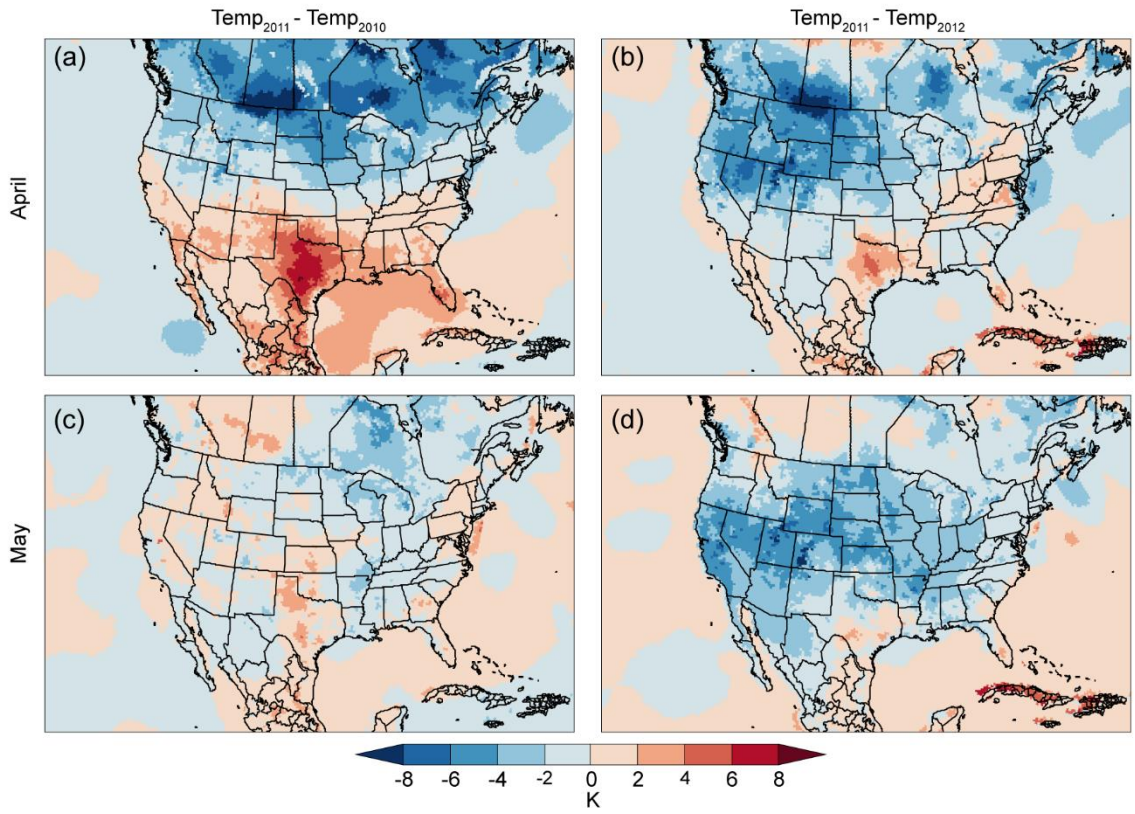

Figure S8 The monthly averaged surface temperature in April and May from 2010 to 2012.

References

Shen, H., Chen, Y., Hu, Y., Ran, L., Lam, S. K., Pavur, G. K., Zhou, F., Pleim, J. E., and Russell, A. G.: Intense Warming Will Significantly Increase Cropland Ammonia Volatilization Threatening Food Security and Ecosystem Health, One Earth, 3, 126-134, https://doi.org/10.1016/j.oneear.2020.06.015, 2020.

Bash, J.O., Cooter, E.J., Dennis, R.L., Walker, J.T., Pleim, J.E.: Evaluation of a regional air-quality model with bidirectional NH_3 exchange coupled to an agroecosystem model. Biogeosciences. 10, 1635-1645, https://doi.org/10.5194/bg-10-1635-2013, 2013.

Comment 12

Page 9, line 277: it may be helpful to also include a priori emission totals in those three months. The posterior emission indicates that the total NH_3 emission decreases linearly from April to July and to October. Then what would the seasonality look like?

Response

In response to this comment, a sentence is added in line 278 to include *a priori* emission totals, and the posterior emission estimates constrained by daily IASI-NH_3 averages are updated as follow: "*The total NH_3 emissions in the optimized estimates are 623 Gg, 564 Gg, and 320 Gg per month in April, July, and October, respectively. In comparison, the emission estimates in the 2011 NEI are 462 Gg, 475 Gg, and 304 Gg per month for the three months.*"

The updated *posterior* emission estimate in April is still the highest. But the difference between emission totals in April and July is much smaller comparing to that between the emission estimates constrained by monthly IASI-NH_3 averages. In comparison, the *a priori* emission estimate in July is slightly higher than that in April. Yet, we cannot draw a confident conclusion on the seasonality of NH_3 emissions due to high uncertainties in NH_3 emission estimates in April. As we suggested in the manuscript (lines 232 – 234, and lines 281 – 284), optimizing NH_3 emissions in April using the inverse modeling technique is more challenging than July and October because of the greater differences in the magnitude and the spatial distribution of the emissions. Better knowledge about agricultural activities and more independent ground and space observations are needed to better constrain the NH_3 emission inventory in the spring months.

Comment 13

Page 9, line 297 and page 12, line 384: it is contradictory to claim that the hybrid inversion "overcomes the over-adjusting problem for high emission rates" and meanwhile attribute the worsening RMSE against AMoN to the emission over-adjustment problem that has supposedly been overcome. Especially the comparison between posterior and AMoN in April (Fig. 4a) seems problematic.

Response

In response to this comment, the sentence in line 297 "*This is likely due to the tendency of satellite-based inversion to over-adjust emissions in high concentration areas (Zhu et al., 2013).*" is deleted. The simulated NH_3 concentration using optimized NH_3 emission estimates agrees better with AMoN observations when daily IASI-NH_3 means instead of monthly means are used as constraints in the 4D-Var inversion. In the updated results, only model evaluation in April shows an obvious increase in NRMSE and a decrease in R^2.

The worsening performance in April is caused by the over-adjustment of NH_3 emissions in Pennsylvania. Using daily means instead of monthly means as constraints help alleviate the over-adjustment. High NH_3 column densities were observed on April 14th and 15th. When daily means are used in the inversion, emissions in other days of the month won't be driven high by these two high observation days. In fact, the posterior emission estimate in Pennsylvania using daily means as constraint is 100% higher than the *a priori* estimates, whereas 700% higher when using monthly means as constraints in the inversion.

The over-adjustment still exists when comparing the simulated surface NH_3 and NH_4^+ concentrations with independent field observations. Although our hybrid method can overcome the over-adjusting problem for high emission areas in the direct 4D-Var method, it tends to over-adjust local emissions when long-range transport dominates the observed high NH_3 column densities. As we mentioned in lines 302 – 303, the hotspot in Pennsylvania on April 14th and 15th possibly came from a large transported plume at high altitude from the central U.S. (Figure S10 and Figure S11). If that was the case, the hybrid inverse modeling framework would have difficulties reproducing the long-range transport contribution for two reasons. First, local emissions in Pennsylvania would be enhanced in the IMB inversion and inter-grid transport were neglected at 216 km by 216 km resolution. Second, the results from such a statistical optimization method are always locally optimal rather than globally optimal. The 4D-Var inversion is more likely to adjust emissions from local and surrounding grid cells instead of grid cells at distance to achieve a local minimum of the cost function. Besides, the IASI-NH_3 column densities may be overestimated because vertical profiles with the highest concentrations near the surface have been assumed in the retrieval process.

The sentences in line 295 – 308 were revised to update the model evaluation results against AMoN observations and better explain the worsening model performance in April, as follow. "*In general, the optimized NH_3 emission reduces the negative NMB when comparing the CMAQ outputs with AMoN NH_3 concentration for all three months. There is a greater improvement at the high concentration end than the low concentration end because both IASI satellite and the passive samplers at the AMoN sites have higher uncertainties in areas with low NH_3 abundance (Van Damme et al., 2015a; Puchalski et al., 2011). Yet, the NRMSE gets higher and R^2 gets lower in April, indicating a higher spatial variation in the residuals. There is an over-adjustment for sites in Pennsylvania in April where there is a hotspot observed by IASI in April 14th and 15th. The hotspot possibly came from a large transported*

*plume at a higher altitude from the central U.S. to Pennsylvania (**Figure S10 and Figure S11**), which is not measured by ground observations at AMoN sites at biweekly resolution. If that is the case, the hybrid inverse modeling framework would have difficulties in reproducing the long-range transport contribution for two reasons. First, local emissions in Pennsylvania would be enhanced in the IMB inversion and inter-grid transport were neglected at 216 km by 216 km resolution. Second, the following 4D-Var inversion very likely reached a local optimal by adjusting emissions from local and surrounding grid cells near the observed hotspot rather than grid cells at distance. Besides, the IASI-NH_3 column densities may be overestimated because vertical profiles with highest concentrations near the surface were assumed in the retrieval process (Whitburn et al., 2016).*"

The limitation is addressed by adding the following sentence in line 315: *"… in most of the CONUS, except in Pennsylvania and surrounding regions in April. The hybrid inverse modeling technique may over-adjust local emissions in hotspots dominated by long-range transport.*"

The sentence in line 385 is also revised as follow: "*The hybrid approach overcomes the over-adjusting problem for high emission areas in the direct 4D-Var method and reduces the computational cost, but it may introduce over-adjustment in special cases where the NH_3 abundance is dominated by transport instead of local emissions.*"

Comment 14

Table 1: the R^2 of 0.08 at other (also the majority of) sites between simulated NH_4^+ and observations in April is bothersome. The N is a reasonably large number (115), so such a low R^2 indicates that the model essentially lost all explanation power after the inversion. The authors are suggested to take a closer look at the April data (for other years than 2011 as well) and make sure they are representative.

Response

When checking the data of Table 1 multiple calculation errors are found. We sincerely apologize for the mistakes. The R^2 at other sites between simulated NH_4^+ and observations in April is 0.26 instead of 0.08.

Both corrected Table 1 for the initial submission version and revised Table 1 based on new optimizing scaling factors are provided below for comparison. The optimized NH_3 emission estimates still exacerbate the high bias in the Pennsylvania state and surrounding areas, but the magnitude is significantly reduced comparing to the initial version. The high IASI-NH_3 observations in April in Pennsylvania state was driven by high retrievals in a few days and using daily means instead of monthly means as constraints helped avoid the artificial high bias in the days without observations. We thank the reviewer again for the critical suggestion.

By comparing the satellite data in different years, we find that IASI-NH_3 column densities in April are higher in 2011 than in 2010 and 2012, however, it is common to have high variations in the column densities in adjacent years and months (Figure S7). We believe the IASI-NH_3 observations in 2011 show a reasonable pattern of NH_3 column densities considering the variations in meteorological conditions and emission activities. The over-adjustment in Pennsylvania and the surrounding region is possibly due to the tendency of this hybrid inverse modeling technique to over-adjust local emissions when long-range transport contributed to the high abundance of NH_3 in that region. Please refer to the response to **Comment 13** for a detailed explanation.

Table 1 (corrected version for initial submission) Statistical summary of the correlation between simulated monthly average NH_4^+ and NO_3^- concentrations and observations in April[a]

NH_4^+	Midwest		Penn		Other	
	a priori	optimized	*a priori*	optimized	*a priori*	optimized
N	47		37		115	
NMB	0.27	0.07	0.00	0.48	-0.35	-0.36
NRMSE	0.40	0.14	0.28	0.42	0.45	0.32

slope	0.52	0.58	0.41	0.32	0.60	0.56
R^2	0.57	0.62	0.24	0.36	0.25	0.26
NO_3^-	Midwest		Penn		Other	
	a priori	optimized	*a priori*	optimized	*a priori*	optimized
N	69		38		240	
NMB	0.64	0.29	0.25	1.40	-0.39	-0.41
NRMSE	0.96	0.66	0.66	1.73	0.63	0.80
slope	0.44	0.50	0.29	0.48	0.62	0.33
R^2	0.76	0.73	0.33	0.67	0.28	0.13

[a] The correlation between observed concentrations and simulated ones based on *a priori* and optimized NH_3 emission estimates are compared. The sites are grouped as the Midwest region, Pennsylvania state and surrounding areas, and other areas.

Table 1 (revised version) Statistical summary of the correlation between simulated monthly average NH_4^+ and NO_3^- concentrations and observations in April[a]

NH_4^+	Midwest		Penn		Other	
	a priori	optimized	*a priori*	optimized	*a priori*	optimized
N	47		37		115	
NMB	0.27	0.22	0.00	0.07	-0.35	-0.35
NRMSE	0.40	0.35	0.28	0.30	0.45	0.44
slope	0.52	0.54	0.41	0.39	0.60	0.65
R^2	0.57	0.65	0.24	0.18	0.25	0.28
NO_3^-	Midwest		Penn		Other	
	a priori	optimized	*a priori*	optimized	*a priori*	optimized
N	69		38		240	
NMB	0.64	0.55	0.25	0.43	-0.39	-0.38
NRMSE	0.96	0.88	0.66	0.73	0.63	0.65
slope	0.44	0.46	0.29	0.29	0.62	0.55
R^2	0.76	0.78	0.33	0.31	0.28	0.25

[a] The correlation between observed concentrations and simulated ones based on *a priori* and optimized NH_3 emission estimates are compared. The sites are grouped as the Midwest region, Pennsylvania state and surrounding areas, and other areas.

Comment 15

Page 10, line 302-303 and page 11, lines 345-346: as CMAQ is a full 3D CTM driven by real WRF meteorology and hourly emissions, those transport should have been captured. Why not?

Response

The hybrid inverse modeling technique is a statistical optimization technique that takes into account the chemistry and physics of the CTM. The system is underdetermined because the model freedom far exceeds the number of satellite observations available. The forward CMAQ model can indeed capture long-range transport with real WRF meteorology and hourly emissions. However, instead of solving for the global optimal, the inversion can adjust emissions from local and surrounding grids instead of grids at distance to achieve a local minimum of the cost function. Besides, in our case of over-adjustment in Pennsylvania, local emissions were enhanced in the IMB inversion and inter-grid transport was neglected at 216 km by 216 km resolution.

It is a limitation of this hybrid inverse modeling method that local emissions may be over-adjusted when the satellite observed hotspots were dominated by long-range transport. The limitation is clarified and addressed in the revised manuscript as follows.

The sentences in lines 300 – 308 are revised as "*There is a greater improvement at the high concentration end than the low concentration end because both IASI satellite and the passive samplers at the AMoN sites have higher uncertainties in areas with low NH_3 abundance (Van Damme et al., 2015a; Puchalski et al., 2011). Yet, the NRMSE gets higher and R^2 gets lower in April, indicating a higher spatial variation in the residuals. There is an over-adjustment for sites in Pennsylvania in April where there is a hotspot observed by IASI in April 14th and 15th. The hotspot possibly came from a large transported plume at a higher altitude from the central U.S. to Pennsylvania (**Figure S10 and Figure S11**), which is not measured by ground observations at AMoN sites at biweekly resolution. If that is the case, the hybrid inverse modeling framework would have difficulties in reproducing the long-range transport contribution for two reasons. First, local emissions in Pennsylvania would be enhanced in the IMB inversion and inter-grid transport were neglected at 216 km by 216 km resolution. Second, the following 4D-Var inversion very likely reached a local optimal by adjusting emissions from local and surrounding grid cells near the observed hotspot rather than grid cells at distance. Besides, the IASI-NH_3 column densities may be overestimated because vertical profiles with highest concentrations near the surface were assumed in the retrieval process (Whitburn et al., 2016).*"

A sentence is added in line 315: *"… in most of the CONUS, except in Pennsylvania and surrounding regions in April. The hybrid inverse modeling technique possibly over-adjusts local emissions in hotspots dominated by long-range transport.*"

Response to Reviewer #2 comments:

Comment 1

This manuscript applied a hybrid inversion approach, which combines a coarse resolution mass balance inversion and a fine-resolution 4D-VAR inversion, to optimize NH_3 emission estimates from the 2011 National emission inventory (2011 NEI) for the U.S. based on the satellite observations of the Infrared Atmospheric Sounding Interferometer NH_3 column density (IASI-NH_3) and the numerical simulations using the CMAQ v5.0 and its multiphase adjoint model. The optimized NH_3 emission inventory suggests the underestimation in the 2011 NEI, especially the NH_3 emission amount in April. The study demonstrated the robustness of the inversed NH_3 emission inventory by evaluating the CMAQ modeling performance of ambient NH_3 concentrations and NH_4^+ wet deposition, analyzed the potential factors accounting to the differences between the NH_3 emissions in 2011 NEI and the optimized estimates, and assessed the influences of the optimized NH_3 emissions to the simulations of ambient aerosol concentrations as well as to the nitrogen deposition exceedances in the U.S. The results are presented in a clear way and the manuscript stands in a good structure. I would recommend publication in Atmospheric Chemistry and Physics after consideration of the following comments.

Response

We thank the reviewer for the comments and valuable suggestions. The detailed responses can be seen below.

Comment 2

Specific comments

1. The adjustment to the a priori emissions of NH_3 is driven by the difference between the observed NH_3 column density and the simulated one, which requires that the uncertainty in the a priori emissions is the dominant explanatory factor for the bias in the simulated NH_3 column density. As we know, several factors other than NH_3 emissions might affect the uncertainty of the simulated NH_3 column density, such as the meteorological fields, the simulated concentrations of other related species, and even other primary emissions. The performance of the WRF model and the CMAQ model in the study are suggested to be introduced in the section 2.3. The influences of these factors on the inversion of NH_3 emissions are also suggested to be discussed in the evaluation of the optimized emission estimates.

Response

We agree with the reviewer that the performance of the inversion will also be influenced by uncertainties and biases in the WRF and the CMAQ model. The model performance of the two models are added in the manuscript as suggested by the reviewer.

The WRF model performance is evaluated by comparing simulated wind speed, temperature, and humidity against surface observations. In general, the WRF simulated meteorological fields agree well with the observations, except for a slight overestimation of wind speed. The CMAQ model performance for simulating gas-particle partitioning of semi-volatile species and reactive nitrogen deposition has been evaluated in detailed in our previous papers using the same input data and model configuration (Chen et al., 2019; Chen et al., 2020). There is a consistent low bias in simulated NH_3 and NH_4^+ concentrations indicating that the NH_3 emission estimates are biased low. Most of the observation-simulation data pairs for $\varepsilon(NH_4^+)$ scatter within the 0.5 to 2 range, and there is no significant systematic bias found in $\varepsilon(NH_4^+)$. Larger biases were found for locations with low relative humidity, low NH_3 and NO_x emissions, or significant dust emissions (Chen et al., 2019). For deposition evaluation, both dry and wet deposition amount are biased low, further indicating a possible low bias in NH_3 emission estimates. Besides, the biases in gas-particle partitioning ratio and precipitation amounts also affect the model performance (Chen et al., 2020). The most relevant evaluations including the gas-particle partitioning of NH_3 and NH_4^+ ($\varepsilon(NH_4^+)$, defined as the molar ratio of NH_4^+ to the sum of NH_3 and NH_4^+), as well as deposition of NH_4^+ are provided in the supporting information.

A sentence describing the WRF model performance is added in line 170 as follows. "*The simulated meteorological fields show good agreement with surface observations (**Figure S2**) (NOAA, 2020).*"

Sentences describing CMAQ model evaluation results are added in line 174, section 2.3, as follows. "*To evaluation CMAQ model performance, the simulated gas-particle partitioning ratio of NH_3-NH_4^+ and NH_4^+ deposition is compared with observations from AMoN, Clean Air Status and Trends Network (CASTNET), and National Atmospheric Deposition Program (NADP) (**Figure S3 and Figure S4**). CMAQ captures the overall spatial pattern of these governing processes for atmospheric NH_3 abundance, considering the uncertainties in emissions, model parameters, and meteorological fields. Expanded evaluation of CMAQ model performance in simulating gas-particle partitioning and nitrogen deposition has been conducted in previous studies (Chen et al, 2019; Chen et al., 2020).*"

Sentences are added in the discussion to address the impacts of uncertainties from the WRF and the CMAQ model as follows.

Sentences are added in line 284 as follows. "*Besides the a priori emission inventory and observational constraints, the inversion performance will also be affected by other processes (e. g., gas-particle partition, transport, cloud and precipitation, and dry and wet deposition) governing the atmospheric abundance of NH_3. Future works refining the pertinent processes will also help improve the optimized NH_3 emission estimates.*"

A sentence is added in line 313 as follows. "*A better representation of the cloud, precipitation, and deposition processes in the WRF and the CMAQ model is needed to close the gap between simulated and observed NH_4^+ deposition amount.*"

Figures showing the WRF and CMAQ performance were added to SI as follows,

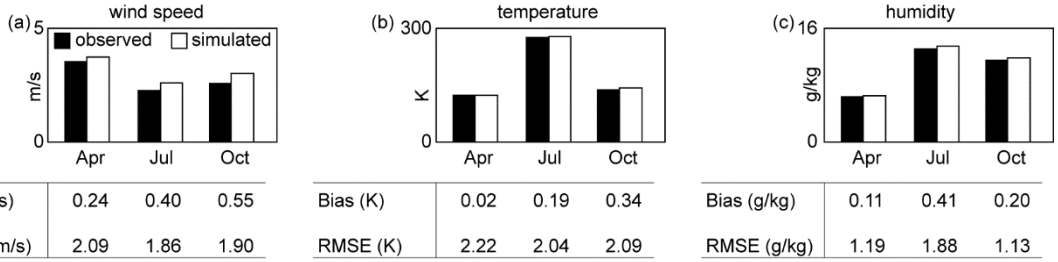

Bias (m/s)	0.24	0.40	0.55
RMSE (m/s)	2.09	1.86	1.90

Bias (K)	0.02	0.19	0.34
RMSE (K)	2.22	2.04	2.09

Bias (g/kg)	0.11	0.41	0.20
RMSE (g/kg)	1.19	1.88	1.13

Figure S2 Model evaluation for WRF simulated meteorological fields against TDL hourly observations for April, July, and October. The bias and RMSE are listed below each plot.

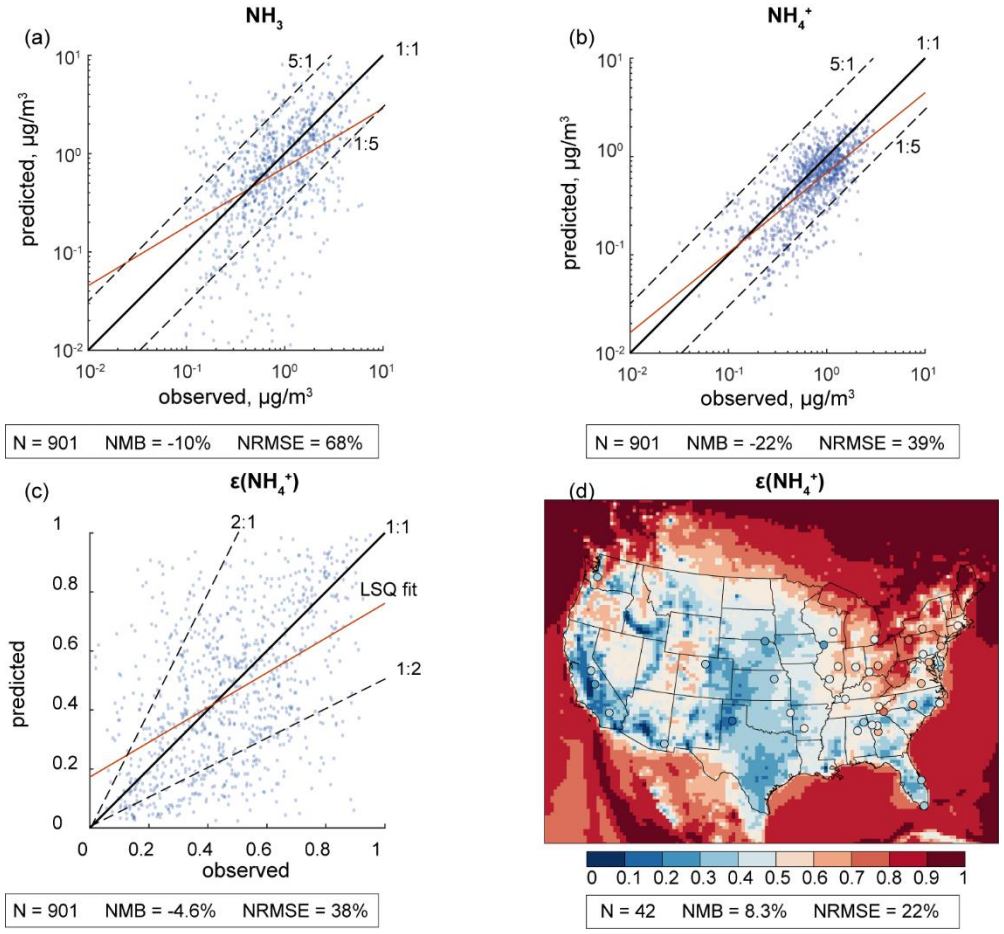

Figure S3 Model evaluation for CMAQ simulated bi-weekly average surface concentrations of NH_3 (a), NH_4^+ (b), and the gas-particle partitioning ratios, $\varepsilon(NH_4^+)$ (c) against observations from collocated AMoN (Ammonia Monitoring Network) and CASTNET (Clean Air Status and Trends Network) sites. Overlay of annual mean $\varepsilon(NH_4^+)$ based on simulated (color map) and observed (colored dots) concentrations are also plotted (d). The 1:1 line (solid black line), data range line (dashed back line with ratio labeled) and regression line (red) is also plotted. Number of data points (N), NMB, and NRMSE are provided along each plot.

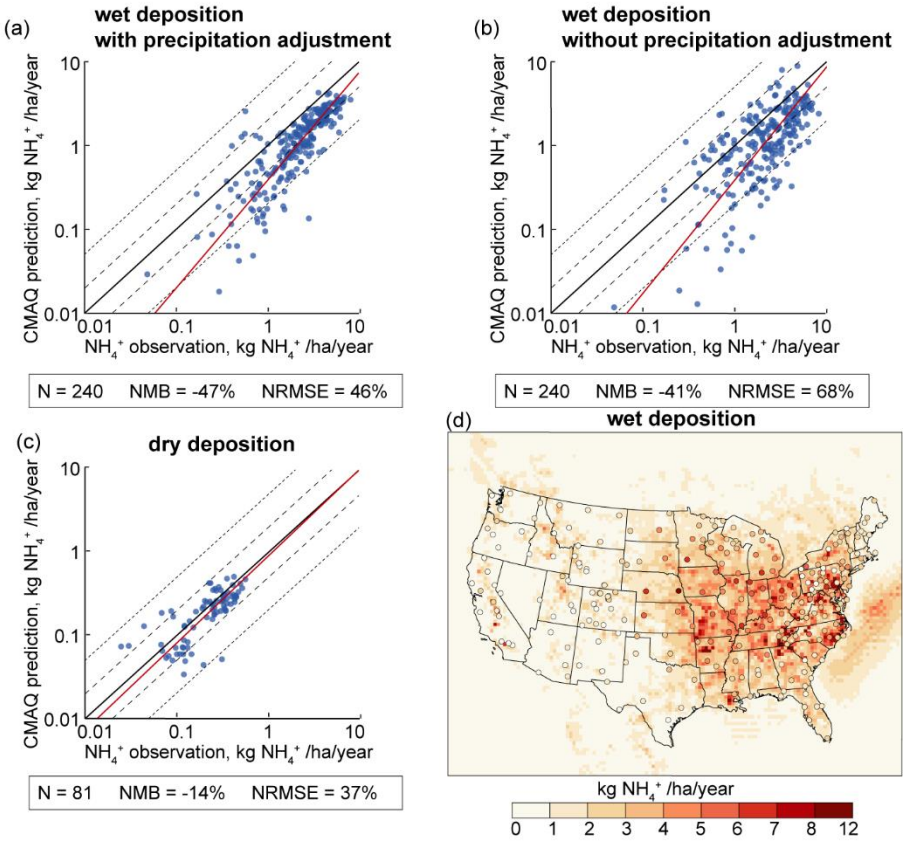

Figure S4 Model evaluation for CMAQ simulated wet (a and b) and dry (c) deposition of NH_4^+ against observations from the NADP (National Atmospheric Deposition Program) and the CASTNET (Clean Air Status and Trends) Network. Overlay of annual NH_4^+ wet deposition based on simulated (color map) and observed (colored dots) amount are also plotted (d). The scatter plots show the comparison between CMAQ predicted and observed annual dry, wet, and total deposition amounts, with the blue line showing the linear regression line. The 1:1 line (solid black line), data range line (dashed back line with ratio labeled) and regression line (red) is also plotted. Number of data points (N), NMB, and NRMSE are provided along each plot. For wet deposition, the CMAQ model performance with (a) and without (b) precipitation adjustment are evaluated.

References

NOAA (2020). Meteorological Development Laboratory/Office of Science and Technology/National Weather Service/NOAA/U.S. Department of Commerce: TDL U.S. and Canada Surface Hourly Observations, Research Data Archive at the National Center for Atmospheric Research, Computational and Information Systems Laboratory, https://rda.ucar.edu/datasets/ds472.0/, 1987. Accessed 24 Dec 2020.

Chen, Y.; Shen, H.; Shih, J.-S.; Russell, A. G.; Shao, S.; Hu, Y.; Odman, M. T.; Nenes, A.; Pavur, G. K.; Zou, Y.; Chen, Z.; Smith, R. A.; Burtraw, D.; Driscoll, C. T.: Greater contribution from agricultural sources to future reactive nitrogen deposition in the United States. Earth's Future, doi: 10.1029/2019EF001453, 2020.

Comment 3

2. In section 3.3, lines 301-306: Do the outputs of the WRF/CMAQ model present the large transported plume from the central U.S. to Pennsylvania on April 14th and 15th? Do other data or analysis (such as wind observations at high altitude, trajectory analysis) support the possibility of this transport?

Response

The spatial pattern of CMAQ simulated NH_3 column density does not present similar patterns observed by the IASI satellite on April 14th and 15th, even using optimized NH_3 emissions as input. This is probably because the optimized results failed to capture long-range transport contribution and over-adjusted local emissions in Pennsylvania.

Although the Atmospheric Infrared Sounder (AIRS) and the Tropospheric Emission Spectrometer (TES) also measures NH_3 column densities in 2011, it is hard to derive daily spatial pattern in the CONUS. For AIRS, only monthly level 3 data has been developed at this moment and the coverage is poor in northeastern U.S. For TES, the satellite swath is too narrow to provide complete daily coverage for CONUS.

In the revision, we performed a trajectory analysis using NOAA HYSPLIT model driven by meteorological fields forecasted by the North American Mesoscale Forecast System (NAM) at 12 km by 12 km resolution. Forward trajectory simulation was performed for April 13th to 15th with a source located in Oklahoma at surface level (37.0 N, 94.7 W). Backward trajectory simulation was performed for April 15th with a receptor located in Pennsylvania (40.9 N, 77.6 W) at both surface level and elevated level (5 km). The forward air parcel trajectories show that long-range transport toward northern and northeastern regions occurred on April 14th and 15th. The backward air parcel trajectories also show that NH_3 in elevated height may came in from the central U.S.

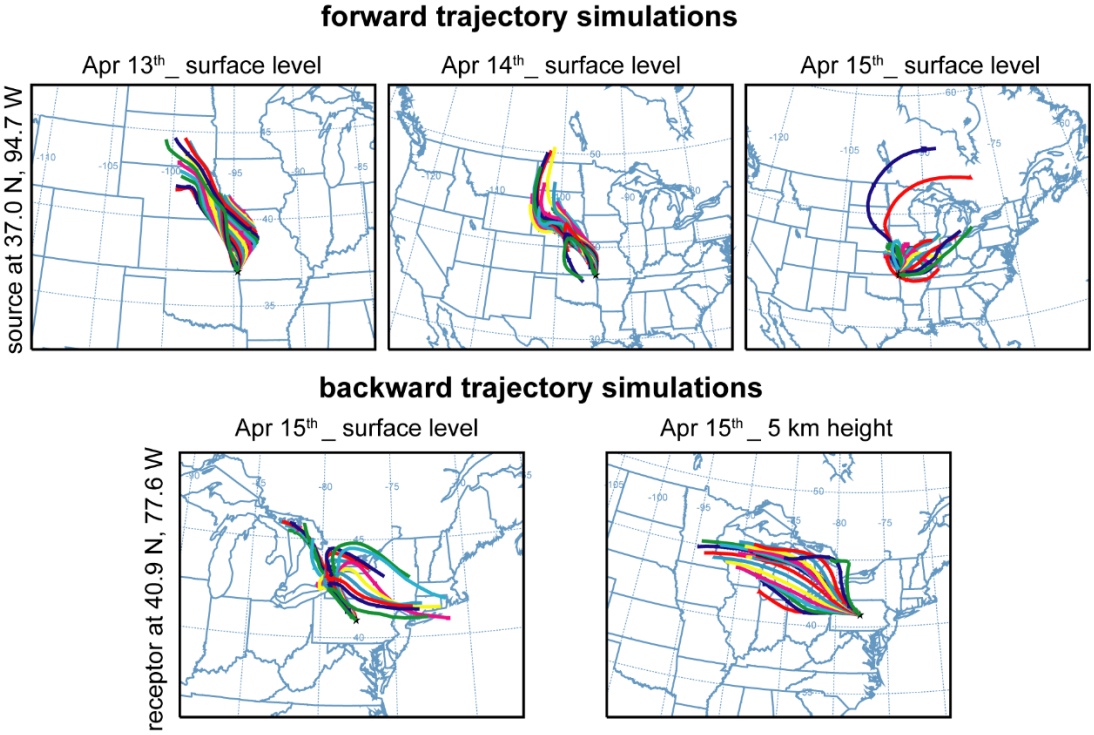

Figure S11 Forward and backward trajectory analysis generated from the NOAA HYSPLIT model. The location of the source (forward) and receptor (backward) are shown as stars in the figures. The starting time of each trajectory is 1 hour apart, from 00:00 to 24:00 local time on each day.

Again, the long-range transport contribution is our speculation based on the IASI-NH_3 spatial distribution. Although the trajectory analysis partially supports our speculation, the high IASI-NH_3 column densities on April 14th and 15th

warrants further investigation. In the revised manuscript, we further clarified that the long-range transport is our hypothesis to explain the discrepancy between IASI-NH_3 and surface observations in Pennsylvania for April 2011.

The sentences in lines 300 – 308 is revised as follows. "*There is an over-adjustment for sites in Pennsylvania in April where there is a hotspot observed by IASI in April 14th and 15th. The hotspot possibly came from a large transported plume at a higher altitude from the central U.S. to Pennsylvania (**Figure S10 and Figure S11**), which is not measured by ground observations at AMoN sites at biweekly resolution. If that is the case, the hybrid inverse modeling framework would have difficulties in reproducing the long-range transport contribution for two reasons. First, local emissions in Pennsylvania would be enhanced in the IMB inversion and inter-grid transport were neglected at 216 km by 216 km resolution. Second, the following 4D-Var inversion very likely reached a local optimal by adjusting emissions from local and surrounding grid cells near the observed hotspot rather than grid cells at distance. Besides, the IASI-NH_3 column densities may be overestimated because vertical profiles with highest concentrations near the surface were assumed in the retrieval process (Whitburn et al., 2016).*"

Figure S11 showing the trajectory analysis results is added to the SI.

Comment 4

3. As shown in Figure 4, the optimized NH_3 emission reduces the negative NMB when comparing the CMAQ outputs with AMoN NH_3 concentrations, but increases the NRMSE and decreases the correlation. In my opinion, the optimized NH_3 inventory does not greatly improve the agreement between CMAQ simulated NH_3 concentrations and the observations. The near ground ambient NH_3 concentrations might reflect more direct signal of the NH_3 emissions than the NH_3 column density. If the ambient NH_3 measurements together with the satellite observations are used to inverse the NH_3 emissions, we would obtain more reasonable optimized emission estimates.

Response

We agree with the reviewer that near ground ambient NH_3 concentration observations might better constrain NH_3 emissions than the satellite NH_3 column densities. However, only 110 active sites are measuring bi-weekly average NH_3 concentration from the AMoN network in the U.S. The ground observations are too sparse to provide useful constraints in the inversion because of the high spatiotemporal heterogeneity of NH_3. Therefore, we decide to leave out the AMoN observations as an independent set of observations to evaluate the robustness of the inversion outcomes. It would be ideal if the two sets of observations can be used together in the inversion if more ground NH_3 observations become available in the future.

The sentence in line 395 is revised as follows: "*…shows that the optimized NH_3 emission estimates reduce the NMB between model outputs and independent observations, especially in April. The NRMSE remains high, indicating 1) the potential to further optimize NH_3 emission estimates when more representative observations of ambient NH_3 abundance becomes available; 2) the need to address the uncertainties in other processes affecting the NH_3 abundance, such as gas-particle partitioning, dry and wet deposition, and in cloud processes.*"

Comment 5

Technical comments

1. In lines 434-436 and lines 541-542: Please add the journals which the references are submitted to.

Response

The two references are updated as follows.

lines 434 – 436:

Cao, H., Henze, D. K., Shephard, M. W., Dammers, E., Cady-Pereira, K., Alvarado, M., Lonsdale, C., Luo, G., Yu, F., Zhu, L., Danielson, C. G., and Edgerton, E. S.: Inverse modeling of NH_3 sources using CrIS remote sensing measurements, Environ Res Lett, 15, 104082, 10.1088/1748-9326/abb5cc, 2020.

lines 541 – 542:

Shen, H., Chen, Y., Hu, Y., Ran, L., Lam, S. K., Pavur, G. K., Zhou, F., Pleim, J. E., and Russell, A. G.: Intense Warming Will Significantly Increase Cropland Ammonia Volatilization Threatening Food Security and Ecosystem Health, One Earth, 3, 126-134, https://doi.org/10.1016/j.oneear.2020.06.015, 2020.

High-resolution Hybrid Inversion of IASI Ammonia Columns to Constrain U.S. Ammonia Emissions Using the CMAQ Adjoint Model

Yilin Chen[1], Huizhong Shen[1], Jennifer Kaiser[1,2], Yongtao Hu[1], Shannon L. Capps[3], Shunliu Zhao[4], Amir Hakami[4], Jhih-Shyang Shih[5], Gertrude K. Pavur[1], Matthew D. Turner[6], Daven K. Henze[7], Jaroslav Resler[8], Athanasios Nenes[9,10], Sergey L. Napelenok[11], Jesse O. Bash[11], Kathleen M. Fahey[11], Gregory R. Carmichael[12], Tianfeng Chai[13], Lieven Clarisse[14], Pierre-François Coheur[14], Martin Van Damme[14], Armistead G. Russell[1]

[1]School of Civil and Environmental Engineering, Georgia Institute of Technology, Atlanta, Georgia 30332, United States

[2]School of Earth and Atmospheric Sciences, Georgia Institute of Technology, Atlanta, Georgia 30332, United States

[3]Department of Civil, Architectural, and Environmental Engineering, Drexel University, Philadelphia, Pennsylvania 19104, United States

[4]Department of Civil and Environmental Engineering, Carleton University, Ottawa, Ontario K1S5B6, Canada

[5]Resources for the Future, Washington, D.C. 20036, USA

[6]SAIC, Stennis Space Center, MS 39529, USA

[7]Mechanical Engineering Department, University of Colorado, Boulder, CO 80309, USA

[8]Institute of Computer Science of the Czech Academy of Sciences, Prague, 182 07, Czech Republic

[9]Institute for Chemical Engineering Sciences, Foundation for Research and Technology Hellas, Patras, GR-26504, Greece

[10]School of Architecture, Civil & Environmental Engineering, Ecole polytechnique fédérale de Lausanne, CH-1015, Lausanne, Switzerland

[11]Atmospheric & Environmental Systems Modeling Division, U.S. EPA, Research Triangle Park, NC 27711, USA

[12]Department of Chemical and Biochemical Engineering, University of Iowa, Iowa City, IA 52242, USA

[13]NOAA Air Resources Laboratory (ARL), Cooperative Institute for Satellites Earth System Studies (CISESS), University of Maryland, College Park, MD 20740, USA

[14]Université libre de Bruxelles (ULB), Spectroscopy, Quantum Chemistry and Atmospheric Remote Sensing (SQUARES), Brussels, Belgium

Correspondence to: Armistead G. Russell (ar70@ce.gatech.edu)

Abstract

Ammonia (NH_3) emissions have large impacts on air quality and nitrogen deposition, influencing human health and the well-being of sensitive ecosystems. Large uncertainties exist in the "bottom-up" NH_3 emission inventories due to limited source information and a historical lack of measurements, hindering the assessment of NH_3-related environmental impacts. The increasing capability of satellites to measure NH_3 abundance and the development of modeling tools enable us to better constrain NH_3 emission estimates at high spatial resolution. In this study, we constrain the NH_3 emission estimates from the widely used national emission inventory for 2011 (2011 NEI) in the U. S. using Infrared Atmospheric Sounding Interferometer NH_3 column density measurements (IASI-NH_3) gridded at a 36 km by 36 km horizontal resolution. With a hybrid inverse modeling approach, we use CMAQ and its multiphase adjoint model to optimize NH_3 emission estimates in April, July, and October. Our optimized emission estimates suggest that the total NH_3 emissions are biased low by ~~32~~26% in 2011 NEI in April with overestimation in Midwest and underestimation in the Southern States. In July and October, the estimates from NEI agree well with the optimized emission estimates, despite a low bias in hotspot regions. Evaluation of the inversion performance using independent observations shows reduced underestimation in simulated ambient NH_3 concentration in all three months and reduced underestimation in NH_4^+ wet deposition in April. Implementing the optimized NH_3 emission estimates improves the model performance in simulating $PM_{2.5}$ concentration in the Midwest in April. The model results suggest that the estimated contribution of ammonium nitrate would be biased high in *a priori* NEI-based assessments. The higher emission estimates in this study also imply a higher ecological impact of nitrogen deposition originating from NH_3 emissions.

1. Introduction

Ammonia (NH_3) emissions play a major role in ambient aerosol formation and reactive nitrogen deposition (Stevens, 2019: Houlton et al., 2013). However, our understanding of NH_3 sources and sinks is limited by the large uncertainties present in the NH_3 emissions inventories (Xu et al., 2019; McQuilling and Adams, 2015). In chemical transport models, uncertainties in NH_3 emissions propagate into the dynamic modeling of the atmospheric transport, chemistry, and deposition of NH_3, other reactive nitrogen species, and other key atmospheric constituents associated with NH_3 (Heald et al., 2012; Paulot et al., 2013; Kelly et al., 2014; Zhang et al., 2018b), hindering an accurate assessment of the various NH_3-related environmental impacts and the associated sources. The large uncertainties in the NH_3 emission inventories are partially due to a lack of sufficient in-situ NH_3 measurements that could be used to constrain emission estimates (Zhu et al., 2015). ~~This work utilizes satellite observations from the Infrared Atmospheric Sounding Interferometer NH_3 column density measurements (IASI-NH_3) (Clarisse et al., 2009;Van Damme et al., 2017), to provide a high-resolution, optimized NH_3 emission inventory for the U.S. developed using an adjoint inverse modeling technique (Li et al., 2019), the robustness of which is demonstrated by evaluation against multiple independent in-situ measurements.~~

Emerging satellite observations of gaseous NH_3 provide a unique opportunity to better constrain the bottom-up NH_3 emission estimates for both their spatial distribution and seasonality. Bottom-up inventories calculate the NH_3 emissions based on estimated activity levels and corresponding emission factors, both of which are subject to high uncertainties, particularly for agricultural sources, the major contributor (Cooter et al., 2012;McQuilling and Adams, 2015). Several studies have utilized NH_3 column density retrieved from the Infrared Atmospheric Sounding Interferometer (IASI)~~from IASI~~ (Clarisse et al., 2009; Van Damme et al., 2015b) or the Atmospheric Infrared Sounder (AIRS; (Warner et al., 2016)) as well as the inferred surface mixing ratio of NH_3 from the Cross-track Infrared Sounder (CrIS; (Shephard and Cady-Pereira, 2015; Shephard et al., 2019)) to characterize the spatiotemporal distribution of NH_3. These satellite measurements are useful for supplementing emission inventories to identify and quantify underestimated or missing emission hotspots, especially in intensive agricultural zones (Van Damme et al., 2018; Dammers et al., 2019; Clarisse et al., 2019). These studies find that the satellite-derived emission estimates are often twice as much as the bottom-up estimates on a regional scale and can be over 10 times higher over hotspots. However, the NH_3 retrievals from satellites are also subject to large uncertainties when the signal-to-noise ratio is low, which limits their ability to accurately measure NH_3 columns in low emission areas (Clarisse et al., 2010; Van Damme et al., 2015a).

Inverse modeling-based optimization combines the information from *a priori* emission inventories and observations and allows us to use the information from both. As one of the inverse modeling methods, the four-dimensional variational assimilation (4D-Var) method seeks the best emission estimate by minimizing a cost function that measures the differences between observations and model predictions, as well as the differences between a prior and adjusted emission estimates. 4D-Var can be computationally expensive at fine model resolutions or with a large set of observations to be assimilated (Brasseur and Jacob, 2017). Recent studies took advantage of the implementation of the adjoint technique in the chemical transport models to conduct 4D-Var for optimizing emissions estimation (Zhu et al., 2013; Paulot et al., 2014; Zhang et al., 2018c). The adjoint-based inversion method calculates the gradients of a cost function analytically and searches the solution using a steepest-descent optimization algorithm through iterating (Brasseur and Jacob, 2017). By testing the performance of the inverse modeling method using artificial observational data, Li et al. (2019) proposed that a two-step optimization process, which combines the iterative mass balance (IMB) method and the 4D-Var method, can further reduce the computational cost. The IMB method assumes a linear relationship between the NH_3 column density and local NH_3 emission and searches the emission scaling factors iteratively until the simulated NH_3 column density converges to the observations. At a coarse (2°×2.5°) resolution, the IMB method is as effective as the 4D-Var method and requires 2/3 less computational time. In the second step, emission scaling factors obtained from the IMB method with a coarser resolution are used as an initial starting point for 4D-Var optimization process to reduce the overall computational time (Li et al., 2019).

This work utilizes satellite observations from the IASI NH_3 column density measurements (IASI-NH_3) (Clarisse et al., 2009;Van Damme et al., 2017), to provide a high-resolution, optimized NH_3 emission inventory for the U.S. developed using an adjoint inverse modeling technique (Li et al., 2019), the robustness of which is demonstrated by

evaluation against multiple independent in-situ measurements. ~~In this study, t~~The IASI-NH_3 dataset was applied to optimize NH_3 emission estimates from the 2011 National Emission Inventory (NEI 2011) using CMAQ and its adjoint model at a 36 km×36 km resolution. The multiphase adjoint model for CMAQ v5.0 was developed recently, including full adjoints for gas-phase chemistry, aerosols, cloud process, diffusion, and advection (Zhao et al., 2019). Both process-by-process and full adjoint model evaluations show reasonable accuracy based on agreements between the adjoint sensitivities and forward sensitivities (Zhao et al., 2019). Previous inversion based NH_3 emission constraint using in-situ measures are limited by the spatial coverage and representativeness of the measurements (Gilliland et al., 2006; Henze et al., 2009; Paulot et al., 2014;). Zhu et al. (2013) first attempted to optimize NH_3 emission inventory using NH_3 derived from the Tropospheric Emission Spectrometer (TES) satellite at 2°×2.5° resolution (Zhu et al., 2013). Inverse modeling at such a coarse resolution is limited to refining regional emissions. Similar to the inversion using CrIS NH3 measurements (Cao et al., 2020), inversion with the IASI-NH_3 dataset allows us to perform the optimization at a finer resolution with its daily global spatial coverage. Besides, the hybrid inversion approach adopted in this study allows us to calculate full adjoint sensitivities online instead of using approximated sensitivities from the ~~offline simulations~~offline simulations (Zhu et al., 2013, Cao et al., 2020). The performance of our optimized estimates and the NEI 2011 are evaluated and compared based on in-situ observed ambient NH_3 concentrations and NH_4^+ wet deposition. Finally, by substituting the *a priori* NH_3 emissions with the optimized emissions, we assess the subsequent changes in simulated ambient $PM_{2.5}$ concentrations and nitrogen deposition exceedances.

2. Materials and Methods

2.1 IASI-NH_3 observations

NH_3 column densities retrieved from IASI onboard the Metop-A satellite are assimilated to constrain spatially-resolved NH_3 emissions using the 2011 NEI as the *a priori* inventory (Clarisse et al., 2009; Van Damme et al., 2014; USEPA, 2014). The polar sun-synchronous satellite has a 12-km diameter footprint at nadir and a bidaily global coverage. Only observations from the morning pass around 9:30 am local standard time (LST) are used due to more favorable thermal contrast and smaller errors comparing to the ones from the night pass around 9:30 pm (LST). A comparison between the IASI-NH_3 data and ground-based Fourier transform infrared observations shows a correlation between the two with r = 0.8 and the slope = 0.73, indicating a tendency of IASI-NH_3 to underestimate the FTIR observations (Dammers et al., 2016). A comparison between IASI-NH_3 and airborne measurements also indicated an underestimation in California, while the comparison between IASI-NH_3 and ground observation from Ammonia Monitoring Network (AMoN) network indicated an overestimation (Van Damme et al., 2015a; NADP, 2014). Overall, the evaluations show broad consistency between IASI-NH_3 and other independent measurements with no consistent biases identified. These evaluations were based on previous datasets. Here we use a new version that relies on another retrieval algorithm, which among other things has a better performance for measurements under unfavorable conditions (Whitburn et al., 2016; Van Damme et al., 2017).

Specifically, the NH_3 products for 2011 from ANNI-NH_3-v2.2R-I datasets were used (Van Damme et al., 2017). The algorithm relies on the conversion of hyperspectral range indices to NH_3 column density using a neural network that takes into account 20 input parameters characterizing temperature, pressure, humidity, and NH_3 vertical profiles. A relative uncertainty estimate is provided along with each of the NH_3 vertical column density in the dataset. Small negative columns are possible – and these are valid observations, needed to reduce overall biases in the dataset. As the retrieval is unconstrained, no averaging kernels are calculated. We therefore directly compare the IASI-NH_3 column density with the simulated column density in CMAQ. Such comparison may be biased because the sensitivity of retrieved NH_3 column densities to NH_3 concentrations is height-dependent (typically peaks around 700 – 850 hPa) (Dammers et al., 2017; Shephard et al., 2015). Although the CMAQ simulated NH_3 columns are also most sensitive to NH_3 concentration changes between 700 to 900 hPa (**Figure S1**), we cannot quantify the relating uncertainties without knowing the averaging kernels. Without information on averaging kernels, differences between NH_3 vertical profiles in CMAQ and the ones used for retrieval may also contribute to the bias between retrieved and modeled column densities, depending on the magnitude of differences (Whitburn et al., 2016).

The NH_3 retrieved columns densities are regridded to the 36-km by 36-km CMAQ grid for 4D-Var data assimilation, and 216-km by 216-km resolution (a 6 grid by 6 grid CMAQ simulation grid matrix) for iterative mass balance (**Figure 1**). The mean column density (Ω_o) is calculated as the arithmetic mean of all retrievals with their centroids falling in the same grid cell, ~~The mean column density (Ω_o) is calculated as the monthly arithmetic mean of all retrievals with their centroids falling in the same grid,~~ following the recommendation that the unweighted mean is preferred for the updated version of IASI-NH_3 as error-weighting can lead to biases (Van Damme et al., 2017). The error (molec/cm^2) corresponding to the mean column density in each grid is calculated as: ~~The relative error (molec/cm^2) corresponding to mean column density in each grid is calculated following Van Damme et al. (2014) as:~~

~~$\bar{\sigma} = \frac{\sum \frac{1}{\sigma_i}}{\sum \frac{1}{\sigma_i^2}} \times \Omega_o$~~ $\bar{\sigma} = \sqrt{\frac{\sum(\sigma_i \times \Omega_i)^2}{n-1}}$

(1)

where $\bar{\sigma}$ is the mean error (molec/cm^2), Ω_i is the NH_3 column density from IASI-NH_3 level 2 data, σ_i is the relative error associated with each Ω_i as reported, n is the number of retrievals within each grid cell during the defined time period. For 4D-Var inversion and IMB inversion, daily and monthly means and errors are calculated, respectively. ~~where $\bar{\sigma}$ is mean relative error (molec/cm^2), σ_i is the relative error associated with each NH_3 column density retrieval as reported, and Ω_o is the mean column density (Van Damme et al., 2014).~~

The observations from April, July, and October are used to constrain the monthly NH_3 emission estimates in corresponding months from 2011 NEI. Limited by the high computational cost of adjoint-model-based inversion, the optimization is only performed for the three months selected instead of a full year. Observations from winter months are not used because they are too noisy when the thermal contrast is low (Dammers et al., 2016).

2.2 NH_3 emission from 2011 NEI

The EPA 2011 NEI is used as *a priori* emission estimates. Major NH_3 sources include livestock waste management, fertilizer application, mobile sources, fire, and fuel combustion, with the majority being emitted by the first two sources. Specifically, the emissions from livestock waste management are estimated based on county-level animal population data and process-based daily emission factors. Emissions from fertilizer applications are estimated based on county-level fertilizer quantities and fixed emission factors, following the CMU ammonia Model (USEPA, 2015). The NH_3 emissions over Mexico and Canada are derived from the simulation results of a fully coupled bi-directional agroecosystem and chemical-transport model (FEST_C_EPIC_CMAQ_BIDI) (Shen et al., ~~2019~~2020). Emissions for other species also come from the 2011 NEI.

2.3 CMAQ and its adjoint

We use the Community Multiscale Air Quality Modeling System (CMAQ) v5.0 (Byun and Schere, 2006; USEPA, 2012) and its adjoint (Zhao et al., 2019), driven by meteorological fields produced from the Weather Research and Forecasting (WRF) Model v3.8.1 with grid nudging using the North American Regional Reanalysis (NARR) dataset (NOAA, 2019). The simulated meteorological fields show good agreement with surface observations (**Figure S2**) (NOAA, 2020). The CB05 chemical mechanism was adopted for gas-phase chemistry (Yarwood et al., 2005). The model implements ISORROPIA-II in the aerosol module (AERO06) to calculate the gas-particle partitioning of NH_3 and NH_4^+ (Fountoukis and Nenes, 2007). The simulation domain covers the contiguous U.S. (CONUS) and part of Canada and Mexico with a 36 km by 36 km horizontal resolution and 13 vertical layers extending up to 14.5 KPa (~16 km) (**Figure 1**). To evaluation CMAQ model performance, the simulated gas-particle partitioning ratio of NH_3-NH_4^+ and NH_4^+ deposition is compared with observations from ~~Ammonia Monitoring Network (~~AMoN~~)~~, Clean Air Status and Trends Network (CASTNET), and National Atmospheric Deposition Program (NADP) (**Figure S3 and Figure S4**). CMAQ captures the overall spatial pattern of these governing processes for atmospheric NH_3 abundance, considering the uncertainties in emissions, model parameters, and meteorological fields. Expanded evaluation of CMAQ model performance in simulating gas-particle partitioning and nitrogen deposition has been conducted in previous studies (Chen et al, 2019; Chen et al., 2020). Monthly simulations are conducted for April, July, and October in 2011 with a 10-day spin-up for each month.

2.4 Hybrid inversion approach

We chose the hybrid inversion approach to combine the advantage of the faster computational speed of the mass balance method and the better optimization performance of the 4D-Var method. The first step is to apply the IMB approach to adjust the *a priori* (2011 NEI) NH_3 emission at 216 km by 216 km resolution (referred as the coarse grid hereafter) based on the ratio between the monthly-averaged observed (Ω_o) and simulated (Ω_a) NH_3 column density at the satellite overpassing time, iteratively. At each iteration, the emission in each grid cell is scaled by the ratio following the equation below,

$$E_t = \frac{\Omega_o}{\Omega_a} \times E_a \quad (2)$$

where E_t and E_a are the new and *a priori* emission estimates, respectively. The method has been described in detail in previous studies (Li et al., 2019; Cooper et al., 2017; Martin et al., 2003). The IMB is applied at the coarse grid so that the NH_3 column will be dominated by the local emissions instead of transport from neighboring grids (Li et al., 2019). The coarse resolution also reduces the uncertainty associated with IASI-NH_3 as the number of retrievals increases in each grid cell. For grid~~s~~ cells with mean relative error larger than 100%, the satellite observations are considered to be too noisy to provide useful constraints and the *a priori* emission estimates are retained. The iteration stops when the normalized mean square error either decreases by less than 10% or begins to increase. The final scaling factor (ε_0) for each grid cell is the multiplication of the scaling factors derived at each iteration and downscaled to 36 km by 36 km resolution by assigning the same value to the 6 by 6 grid matrix. This scaling factor is applied to the 2011 NEI emissions to create the revised *a priori* estimate for the 4D-Var inversion.

Next, the 4D-Var inversion is performed. The solution of the optimization problem is sought iteratively by minimizing the cost function (J) defined as the combination of error-weighted, squared difference between emission scaling factor and unity and the error weighted, squared difference between IASI-NH_3 and the simulated column density, as below:

$$\mathrm{J} = \gamma(\varepsilon - \varepsilon_0)^T S_a^{-1}(\varepsilon - \varepsilon_0) + (\Omega_o - \mathrm{F}(\varepsilon))^T S_o^{-1}(\Omega_o - \mathrm{F}(\varepsilon)) \quad (3)$$

ε is the monthly emission scaling factor to be optimized at each iteration where $\varepsilon = \log\left({}^{E_t}/_{E_a}\right)$ on the 36 km by 36 km CMAQ grid, consisting of 6104 elements overland grid cells in CONUS. S_a and S_o are error covariance matrices for the *a priori* emission estimates and IASI-NH_3 retrievals, respectively. With limited information on the spatial correlation of the error covariance, the two matrices are assumed to be diagonal (Paulot et al., 2014; Zhu et al., 2013).~~The two matrices are assumed to be diagonal.~~ For S_o, the grid average absolute error is used to represent the observational error. ~~To reduce the influence of retrievals close to or below the detection limit, an estimated detection limit of 4.8×10^{15} molecules/cm^2 is added to the S_o (Dammers et al., 2019).~~ Our test shows that negative Ω_o will lead to a continuous decrease in the adjusted emission for the grid cell because modeled column density cannot become negative. To limit the influence of these negative Ω_o, their original weights are multiplied by 0.01. For S_a, the uncertainty in each grid cell is assumed to be 100% of the *a priori* emissions. F(ε) is CMAQ simulated NH_3 column density sampled at the satellite passing time if there is at least one IASI-NH_3 retrieval in that grid cell; γ is the regularization factor balancing the relative contribution of the *a priori* emission inventory and IASI-NH_3 retrievals to the J value. γ is chosen to be 800 for April and 500 for July and October~~30 for all 3 months~~ based on the L-curve criteria (Hansen, 1999) (**Figure ~~S2~~S5**).

The gradients of the cost function to NH_3 emissions are calculated by the CMAQ adjoint model. In each iteration, the emission-weighted monthly averaged sensitivities in each grid cell are supplied to the L-BFGS-B optimization routine contained in the "optimr" package in R to find the scaling factors that will achieve the minimum of the cost function (Zhu et al., 1997; Byrd et al., 1995). NH_3 column density is re-simulated using adjusted emissions by the

new set of scaling factors. The iteration process is terminated when the decrease in J is less than 2% or the local minimum is reached (Li et al., 2019; Zhu et al., 2013).

2.5 Posterior evaluation

The posterior emissions are evaluated by comparing the model simulation from optimized emissions with observations. Simulated results are compared with ambient NH_3 concentrations from the AMoN (NADP, 2014), and the NH_4^+ wet deposition from the ~~National Atmospheric Deposition Program~~NADP (NADP, 2019). The simulated NH_3 concentration in ppmV is converted to $\mu g/m^3$ using local temperature and pressure from the model meteorological inputs. For evaluation against the NH_4^+ wet deposition, the simulated deposition is scaled by the ratio between measured and simulated precipitation to eliminate the bias introduced by precipitation fields (Appel et al., 2011).

3. Results

3.1 Optimization performance evaluation

The optimized NH_3 emissions reduce the bias in the NH_3 columns between the satellite observation and the model prediction as shown by the decrease in the values of normalized root mean square error (NRMSE) and normalized mean biases (NMBs) in **Figure 2**. There are negative biases using 2011 NEI in all three months, especially in areas with high emission rates. Although the IMB inversion can lower the NRMSE, it tends to over-adjust and introduce a positive bias likely because of the coarse resolution and neglect of the impact of transport. The 4D-Var inversion effectively decreases the positive bias and further reduces the NRMSE. The cost function value reduces by ~~50~~85%, ~~57~~46%, and ~~34~~38% with the 4D-Var inversion in April, July, and October, respectively. We find that it is more challenging to adjust the emissions in April than in the other two months because of the greater differences in the magnitude and the spatial distribution of the emissions. The optimized NH_3 emission successfully captures the high NH_3 column density in the Southern States (Texas and Oklahoma), reducing the NRMSE by ~~98~~half ~~%~~ in that region. Despite the general improvement in the model performance, negative biases in July increase in California's San Joaquin Valley. Scaling up the emission in the San Joaquin Valley will result in high NH_3 concentrations downwind even when the local NH_3 emissions downwind are zeroed, whereas the IASI-NH_3 observed concentrations downwind are low. The transported hotspot downwind of the San Joaquin Valley in CMAQ only occurs in July, suggesting near field removal may not be captured at the current resolution, and warrants further investigation. Grid by grid comparison between model-simulated NH_3 column density using the *a priori* and optimized estimates with IASI-NH_3 shows improved agreement in both high and low emission grid cells after optimization (**Figure ~~S3~~S6**). It shows that the hybrid inversion approach can alleviate the weakness of direct 4D-Var inversion which tends to over-adjust high emission regions and under-adjust low emission regions, mainly because the IMB inversion provides a better initial state.

The IMB inversion took three iterations to achieve the convergence condition for each month, and subsequently, the 4D-Var inversion took ~~five~~ten, four, and ~~three~~ six iterations for April, July, and October, respectively. Fewer iterations are needed with the hybrid approach than the direct 4D-Var inversion which typically takes up to 15 to 20 iterations of adjoint simulation (Paulot et al., 2014; Zhang et al., 2018a). The CPU time of a forward simulation is only 1/5 of an adjoint simulation. In total, the CPU time required by the hybrid approach is expected to be ~~60%~~1/3 to 2/3 lower than the direct 4D-Var inversion approach.

3.2 Optimized estimate of NH_3 emissions

The monthly total NH_3 emission in CONUS increases by ~~46~~35% in April, ~~6.6~~18% in July, and ~~6.9~~10% in October for the optimized estimates, respectively. Spatially, the distribution for high emission regions shifts from Midwest in the 2011 NEI to the Southern States in the optimized estimates in April, whereas the hot spot regions remain consistent in July and October (**Figure 3**). Regional total emissions are summarized according to the USDA Farm Production regions, which defines the areas with similar crop production activities (Cooter et al., 2012). In general, the regional variation of NH_3 emissions in April is dominated by fertilizer application. The optimized estimates in the Corn Belt and Lake States regions are lower than the 2011 NEI, ~~with~~ where high contributions from fertilizer applications were estimated ~~in 2011 NEI, including the Corn Belt, Lake States, and Northern Plains, are lower than the 2011 NEI~~. In contrast, the optimized estimates are 2 – 3 times higher than the 2011 NEI estimates in the Delta States and Southern States where the *a priori* estimates for NH_3 emission from fertilizer application are low. The higher NH_3 emission estimates in the southern states are driven by the enhanced NH_3 column densities from IASI over that region. IASI-NH_3 column densities are higher in 2011 than those in adjacent years (**Figure S7**), which coincides with the higher surface temperature observed in 2011 (NOAA 2019)(**Figure S8**). NH_3 emission will increase due to enhanced NH_3 volatilization from agricultural lands under warmer conditions (Bash et al., 2013; Shen et al., 2020). In fact, the optimized NH_3 emission pattern in April is more consistent with the spatial pattern of inorganic nitrogen fertilizer estimated based on plant demand (Cooter et al., 2012). NH_3 emission in 2011 estimated by CMAQ with NH_3 bidirectional exchange model also predicted higher NH_3 emission in the southern states (Shen et al., 2020). The ratio between NH_3 emission estimates in southern states and that within CONUS is 26% and 18% in the optimized estimates and estimates including NH_3 bidirectional exchange, respectively. In comparison, the ratio is only 10% in the *a priori* NEI estimates, suggesting a potential low bias in 2011 NEI.~~The optimized NH_3 emission pattern in April is more consistent with the spatial pattern of inorganic nitrogen fertilizer estimated based on plant demand (Cooter et al., 2012) as well as the livestock population distribution (USDA, 2012), suggesting the potential bias in the agricultural practices used in 2011 NEI.~~ In July, regional differences are smaller except for the Northern Plain and ~~Southeast~~Mountain region. In the Northern Plain, the NH_3 emission is 66% higher in the optimized estimates, driven by the emission increase in hotspot areas with concentrated animal feeding operations (CAFO) (USDA, 2012; Van Damme et al., 2017, Clarisse et al., 2019). The potential bias in different sectors suggests the need for sectoral inversion when a larger observational dataset becomes available in the future.~~. In the Southeast, the IASI-NH_3 column densities are very low, even over known CAFO sites, and had high errors~~

~~associated with the retrievals because of the low thermal contrast and a smaller number of retrievals (Schiferl et al., 2014).~~ ~~The negative increment in the Pacific region is due to the disagreement between modeled high NH_3 columns and observed low values from IASI NH_3 downwind of the San Joaquin Valley of California, as discussed previously.~~ In October, the relative difference is less than 10% in most of the regions, indicating that the 2011 NEI appropriately reflects the NH_3 emission pattern. There is a significant increase in the NH_3 emissions in Mexico during all three months. Such an emission increment is crucial to improving the model performance in both Mexico and the southwestern U. S. However, it was not a goal of this study to determine emissions biases in Mexico given the limited information on NH_3 emissions.

The total NH_3 emissions in the optimized estimates are ~~671~~ 623 Gg, ~~500~~ 564 Gg, and ~~320~~ 335 Gg per month in April, July, and October, respectively. In comparison, the emission estimates in the 2011 NEI are 462 Gg, 475 Gg, and 304 Gg per month for the three months. Similar to a bottom-up agricultural NH_3 emission inventory (MASAGE_NH_3) and two inverse model optimized estimates based on NH_4^+ wet deposition, we find a higher emission in the spring season (Paulot et al., 2014; Gilliland et al., 2006), while others, including the NEI, estimates a summertime peak (Zhu et al., 2013; USEPA, 2015; Cooter et al., 2012, Cao et al., 2020). The large variation between different inventories warrants both improved information on bottom-up inventories and more observations to support inverse model optimization in the spring season. Better knowledge about agricultural activities and more independent ground and space observations are needed. Besides the *a priori* emission inventory and observational constraints, the inversion performance will also be affected by other processes (e. g., gas-particle partition, transport, cloud and precipitation, and dry and wet deposition) governing the atmospheric abundance of NH_3. Future works refining the pertinent processes will also help improve the optimized NH_3 emission estimates. It should also be noted that there are interannual variations in emission inventories developed for different years. ~~The total emission estimates in July and October are closer to the 2011 NEI estimates than those estimates from other emission inventories and inverse analysis.~~ The good spatial agreement with IASI-NH_3 indicates that the 2011 NEI captures the NH_3 emission pattern in general in these two months. Although the inversion is only applied for the three selected months, the simulated NH_3 column densities using the *a priori* inventory are consistently lower than the IASI-NH_3 observations in 2011 (**Figure S9**), suggesting that the NH_3 emission estimates in 2011 NEI may be biased low in other months, too.

3.3 Evaluation of the optimized emission estimates against independent datasets

The robustness of the NH_3 emission optimization is evaluated by comparing the model outputs using both the *a priori* and optimized emission estimates with independent observations. The bias and uncertainties inherited in the CMAQ forward model and its adjoint, as well as the assumptions made about the uncertainties of the *a priori* emission inventory and IASI-NH_3 observations, will all influence the robustness. Here, we choose to evaluate the outputs against 1) biweekly average ambient NH_3 concentrations measured by AMoN; 2) weekly average NH_4^+ wet deposition measured by NADP (**Figure 4**).

In general, the optimized NH_3 emission reduces the negative NMB when comparing the CMAQ outputs with AMoN NH_3 concentration for all three months. There is a greater improvement at the high concentration end than the low concentration end because both IASI satellite and the passive samplers at the AMoN sites have higher uncertainties in areas with low NH_3 abundance (Van Damme et al., 2015a; Puchalski et al., 2011). Yet, the NRMSE gets higher and R^2 gets lower in April, indicating a higher spatial variation in the residuals. There is an over-adjustment for sites in Pennsylvania in April where there is a hotspot observed by IASI in April 14th and 15th. The hotspot possibly came from a large transported plume at a higher altitude from the central U.S. to Pennsylvania (**Figure S10 and Figure S11**), which is not measured by ground observations at AMoN sites at biweekly resolution. If that is the case, the hybrid inverse modeling framework would have difficulties in reproducing the long-range transport contribution for two reasons. First, local emissions in Pennsylvania would be enhanced in the IMB inversion and inter-grid transport were neglected at 216 km by 216 km resolution. Second, the following 4D-Var inversion very likely reached a local optimal by adjusting emissions from local and surrounding grid cells near the observed hotspot rather than grid cells at distance. Besides, the IASI-NH_3 column densities may be overestimated because vertical profiles with highest concentrations near the surface were assumed in the retrieval process (Whitburn et al., 2016).~~In general, the optimized NH_3 emission reduces the negative NMB when comparing the CMAQ outputs with AMoN NH_3 concentration for all three months. Yet, the NRMSE gets higher and R^2 gets lower in April, indicating a higher spatial variation in the residuals. This is likely due to the tendency of satellite-based inversion to over-adjust emissions in high-concentration areas (Zhu et al., 2013). There is a greater improvement at the high concentration end than the low-concentration end because both IASI satellite and the passive samplers at the AMoN sites have higher uncertainties in areas with low NH_3 abundance (Van Damme et al., 2015a; Puchalski et al., 2011). There is an over-adjustment for sites in Pennsylvania in April where there is a hotspot observed by IASI. The hotspot in monthly average is dominated by high NH_3 column densities observed in April 14th and 15th, possibly from a large transported plume from the central U.S. to Pennsylvania (**Figure S4**). The fact that it is transported at higher altitude in 2 days could explain that it is not measured by ground observations at AMoN sites at biweekly resolution. The long-range transport at higher altitude may lead to an overestimation in IASI retrieved NH_3 column densities which assume a vertical profile with highest concentrations near the surface (Whitburn et al., 2016). Such transport is also not well represented in the hybrid inverse modeling approach where the transport effect is not included in the IMB inversion at 216 km by 216 km resolution.~~

For evaluation against NADP observations, there is a noticeably improved agreement in April with reduced negative NMB and reduced discrepancies for most of the data pairs. For July, the emission optimization only slightly improved the model performance. For October, the optimization increased the NMB from -1.8% to ~~10~~4.8%. It indicates that NH_3 emission is not the dominant explanatory factor for bias in simulated NH_4^+ wet deposition that is commonly observed in chemical transport models (Appel et al., 2011; Paulot et al., 2014). A better representation of the cloud, precipitation, and deposition processes in the WRF and the CMAQ model is needed to close the gap between simulated and observed NH_4^+ deposition amount. Overall, the improved model operational performance for ambient NH_3 suggests that the inverse model optimization applied in this study provides improvements in the NH_3 emission estimates during all three months in most of the CONUS, except in Pennsylvania and surrounding regions

in April. The hybrid inverse modeling technique may over-adjust local emissions in hotspots dominated by long-range transport.

4. Implications

4.1 Ambient aerosol concentration

As a major precursor of ambient aerosol formation, the NH_3 emission inventory is believed to be a major source of uncertainty in $PM_{2.5}$ assessment in several parts of the CONUS (Henze et al., 2009; Schiferl et al., 2014; Heald et al., 2012), which can further bias the source contribution assessments on $PM_{2.5}$-related health impacts (Lee et al., 2015, Zhao et al., 2019). Comparison of the simulated $PM_{2.5}$ mass concentration using the *a priori* and optimized NH_3 emission estimates shows that the NH_3 emission bias in April is a major factor for bias in the modeled $PM_{2.5}$ concentration leading to high or low bias in ammonium nitrate (NH_4NO_3) formation (**Figure 5**). The relative change of the monthly average $PM_{2.5}$ concentration is over ~~10~~5% in one-fifth of the CONUS, including an increase in the Northeastern, Pacific West, ~~and~~ Rocky Mountains regions, part of Texas, and Gulf coast region, and a decrease in the Midwest. For most of these regions, over 90% of the change is driven by the change in concentration of NH_4^+ and NO_3^-.

Comparison of the simulated monthly average NH_4^+ and NO_3^- concentration using the *a priori* estimates against ambient monitoring network data (USEPA, 2018) shows that there is a high bias in the Midwest region and Pennsylvania state, and underestimation low bias for the rest of the sites (**Table 1**). Simulations using the optimized NH_3 emission estimates reduce the high bias in the Midwest region but exacerbate the high bias in the Pennsylvania state and surrounding areas. For the other sites, the impact of optimization is mixed but minor in general.

For the Midwest, our optimized NH_3 emission is ~~31~~12% lower than the 2011 NEI, leading to a ~~20~~ 5 - 30% decrease in NH_4^+ and NO_3^- concentration. Overestimation of NO_3^- in the Midwest has been recognized in previous model evaluations. Previous studies attempted to moderate the high bias by lowering the nitric acid (HNO_3) concentration through either lowering both daytime and nighttime HNO_3 formation rate or raising deposition removal rate (Heald et al., 2012; Zhang et al., 2012; Walker et al., 2012). It was found that such modification in the model parameterization cannot fully account for the overestimation (Heald et al., 2012; Zhang et al., 2012; Walker et al., 2012). Our study implies that the springtime overestimation can partly be explained by the overestimation in NH_3 emissions which drives the high bias in NH_4NO_3 formation.

The large increase of the NH_4NO_3 concentration in Pennsylvania state and surrounding areas is due to the over-amplified local NH_3 emissions in the optimized estimates to match the high NH_3 column density in IASI-NH_3 2011, as discussed earlier. It ~~adds to the existing overestimation in~~leads to higher magnitude of biases in NH_4^+ and ~~NH_4^+~~ ~~and~~ NO_3^- concentration as compared to ground measurements. The fact that the simulated ambient NH_3 concentration, NH_4^+ concentration, and NH_4^+ wet deposition using the optimized NH_3 estimates is biased high in

comparison with independent ground measurements suggests the enhanced NH_3 abundance observed from IASI ~~is~~is possibly driven by long-range transport at higher altitudes instead of local surface emissions.

For the rest of the CONUS, there is only a slight impact of the optimization on simulated NH_4NO_3 formation. For example, although the NH_3 emission is doubled in the San Joaquin Valley in California, the modeled NH_4^+ and NO_3^- concentrations are still biased low using the optimized estimates. A sensitivity test using GEOS-Chem shows that the San Joaquin Valley region is nitric acid-limited instead of ammonia-limited (Walker et al., 2012), suggesting that there is an underestimation in HNO_3 formation. A comparison of the simulated and measured speciated $PM_{2.5}$ shows that there is a low bias in non-volatile cation concentrations in the sites in the San Joaquin Valley, limiting the formation of NH_4NO_3 through gas-particle partitioning (Chen et al., 2019). Thus, attempts to close the gap between the simulated and monitored NH_4^+ and NO_3^- concentrations by scaling NH_3 emission alone are ineffective and might lead to an overestimation in local NH_3 emissions.

For July and October, there is a very limited difference between the simulated $PM_{2.5}$ concentration using the optimized and *a priori* NH_3 emission estimates, as expected, because the change in NH_3 emission is ~~small~~minor. There are only 1% and 4% of the CONUS with a relative change in $PM_{2.5}$ concentration over ~~10~~5%. This result shows that the uncertainty in NH_3 emission estimates is moderate and is not a major contributor to biases in modeled $PM_{2.5}$ in July and October.

4.2 Reactive nitrogen (Nr) deposition

The uncertainties in NH_3 emission inventory also impact the reactive nitrogen (Nr) deposition assessment, which informs the ecosystem impacts evaluation and effective mitigation actions (Ellis et al., 2013). To evaluate the impact of the NH_3 emission optimization on simulated Nr deposition, the Nr deposition amount simulated using optimized and *a priori* emission estimates is analyzed in all biodiversity-protected areas designated by the USGS (**Figure ~~S5~~S12**) within CONUS (USGS, 2018). In total, the Nr deposition increased by ~~39~~27%, ~~2~~9%, and ~~9~~5% on average in these protected areas in April, July, and October, respectively. A regional comparison based on the Level I ecoregions (Pardo et al., 2015) shows that the deposition increment is the highest in the ~~Great Plain region~~Tropical Wet Forests (+~~73~~64%), followed by the ~~Eastern Temperate Forest~~Great Plain region (+~~41~~46%) in April (**Figure 6**). Although the overall increase is small in July and October, the increment can be high in individual ecoregions, including Southern Semiarid Highlands (+~~109~~95% in July) and ~~,~~Temperate Sierras (+~~66~~62% in July)~~, and Marine West Coast (+64% in October).~~ In addition to the increment in deposition amount, higher NH_3 emission, especially in intensive agriculture regions, may indicate higher source contribution from agricultural NH_3 than previous estimates (Lee et al., 2016).

Driven by the increase in the reduced form of Nr (NH_3 and NH_4^+) deposition, a higher share of reduced form of Nr to the total Nr deposition is found in most of the ecoregions for all three months than the NEI-based estimates. More detrimental impacts on sensitive species and biodiversity are expected when this change in dominant Nr form are

considered in addition to the increase in magnitude because the growth of many sensitive plant species will be inhibited by a high NH_4^+ to NO_3^- ratio in soil and water (Bobbink and Hicks, 2014).

5. Conclusions

We apply the newly developed multiphase adjoint of the CMAQ v5.0 chemical transport model and NH_3 column observations from the satellite-borne IASI to optimize NH_3 emissions estimates in the CONUS using a hybrid inversion modeling approach. The approach consists of a coarse-resolution iterative mass balance inversion (216 km by 216 km) and a fine-resolution 4D-VAR inversion (36 km by 36 km) and is performed using IASI-NH_3 observations in April, July, and October. The hybrid approach overcomes the over-adjusting problem for high emission areas in the direct 4D-Var method and reduces the computational cost~~.~~, but it may introduce over-adjustment in special cases where the NH_3 abundance is dominated by transport instead of local emissions.

We use the NH_3 emission from 2011 NEI commonly used in regional and national simulations and assessments as the *a priori* emission. We find that the optimized NH_3 emission inventory differs greatly with the 2011 NEI in April. The emission in Midwest is overestimated and the emission in Southern states is underestimated in the 2011 NEI. Overall, the optimized emission is ~~46~~35% higher in April. The optimized emission estimates in July and October are ~~slightly~~ also higher (~~6.6~~18% and ~~6.9~~10%) than the 2011 NEI estimates ~~and~~ but the spatial distribution agrees well. The IASI-NH_3 observations indicate a consistent underestimation of NH_3 emissions in California's San Joaquin Valley in all three months, however, the inverse modeling fails to properly scale up the emissions in July. The evaluation of simulation outputs against ground measurements including ambient NH_3 concentrations from AMoN and NH_4^+ wet deposition from NADP shows that the optimized NH_3 emission estimates ~~improve the agreement~~reduce the NMB between model outputs and independent observations, especially in April. The NRMSE remains high, indicating 1) the potential to further optimize NH_3 emission estimates when more representative observations of ambient NH_3 abundance becomes available; 2) the need to address the uncertainties in other processes affecting the NH_3 abundance, such as gas-particle partitioning, dry and wet deposition, and in cloud processes.

Application of the optimized NH_3 emission estimates also yields a better agreement between the simulated and observed $PM_{2.5}$ concentration in April in the Midwest region by improving the model performance on simulated NH_4^+ and NO_3^-. It is consistent with previous findings that the uncertainty in NH_3 emission is a key factor limiting the model performance of $PM_{2.5}$. The optimized NH_3 emission estimates in general increase the Nr deposition amount and the relative importance of reduced form Nr, highlighting the importance of constraining NH_3 emission estimates for accurately assessing nitrogen deposition and ecosystem health over sensitive regions.

Data availability. The IASI/Metop-A NH_3 total column Level 2 data is available at the IASI portal provided by the AERIS data infrastructure (ULB, 2018). Independent observations for evaluation including surface NH_3

concentrations, NH_4^+ wet depositions, and speciated $PM_{2.5}$ concentrations are available from the NADP website and Air Quality System (NADP, 2019, 2014; USEPA, 2018).

Author contribution. AR and YC conceived the study. YC, AR, HZ, and JK contributed to the design the method. YC conducted the inverse modeling and data analysis. LC, PFC and MVD are responsible for the IASI NH3 data. SC, SZ, AH, MR, MT, DH, PP, JR, AN, AP, SN, JB, KF, GC, CS, TC, AR developed the adjoint model of CMAQ. YC prepare the manuscript, with discussions and comments from HS, AR, JK, YH, SC, SZ, JS, and GP. All authors have given approval to the final version of the manuscript.

Competing interests. The authors declare that they have no conflict of interest.

Disclaimer. Contents of this publication are solely the responsibility of the grantee and do not necessarily represent the official views of the supporting agencies. Further, the US government does not endorse the purchase of any commercial products or services mentioned in the publication.

Acknowledgments

This publication was made possible by funding from the US EPA under grants R83588001, NASA under grant NNX16AQ29G, and China Scholarship Council (CSC) Grant #201606010393. The authors acknowledge the AERIS data infrastructure for providing access to the IASI data in this study. ULB has been supported by the Belgian State Federal Office for Scientific, Technical and Cultural Affairs (Prodex arrangement IASI.FLOW). L.C. and M.V.D are respectively research associate and postdoctoral researcher with the Belgian F.R.S-FNRS.

References

Appel, K. W., Foley, K. M., Bash, J. O., Pinder, R. W., Dennis, R. L., Allen, D. J., and Pickering, K.: A multi-resolution assessment of the Community Multiscale Air Quality (CMAQ) model v4.7 wet deposition estimates for 2002-2006, Geosci. Model Dev., 4, 357-371, https://doi.org/10.5194/gmd-4-357-2011, 2011.

Bash, J.O., Cooter, E.J., Dennis, R.L., Walker, J.T., Pleim, J.E.: Evaluation of a regional air-quality model with bidirectional NH_3 exchange coupled to an agroecosystem model. Biogeosciences. 10, 1635-1645, https://doi.org/10.5194/bg-10-1635-2013, 2013.

Bobbink, R., and Hicks, W. K.: Factors affecting nitrogen deposition impacts on biodiversity: an overview, in: Nitrogen deposition, critical loads and biodiversity, edited by: Sutton, M. A., Mason, K. E., Sheppard, L. J., Sverdrup, H., Haeuber, R., and Hicks, W. K., Springer Netherlands, Dordrecht, 127-138, 2014.

Brasseur, G. P., and Jacob, D. J.: Modeling of atmospheric chemistry, Cambridge University Press, 520-525, 2017.

Byrd, R. H., Lu, P., Nocedal, J., and Zhu, C.: A limited memory algorithm for bound constrained optimization, SIAM J. Sci. Comput., 16, 1190-1208, https://doi.org/10.1137/0916069, 1995.

Byun, D., and Schere, K. L.: Review of the governing equations, computational algorithms, and other components of the models-3 Community Multiscale Air Quality (CMAQ) modeling system, Appl. Mech. Rev., 59, 51-77, https://doi.org/10.1115/1.2128636, 2006.

Cao, H., Henze, D. K., Shephard, M. W., Dammers, E., Cady-Pereira, K., Alvarado, M., Lonsdale, C., Luo, G., Yu, F., Zhu, L., ~~Bash, J., Rao, V., and~~ Danielson, C. G., and Edgerton, E. S.: Inverse modeling of NH3 sources using CrIS remote sensing measurements, Environ. Res. Lett., 15, 104082, 10.1088/1748-9326/abb5cc, 2020 ~~(under review), 2020~~.

Chen, Y., Shen, H., and Russell, A. G.: Current and future responses of aerosol ph and composition in the U.S. to declining SO_2 emissions and increasing NH_3 emissions, Environ. Sci. Technol., 53, 9646-9655, https://doi.org/10.1021/acs.est.9b02005, 2019.

Chen, Y.; Shen, H.; Shih, J.-S.; Russell, A. G.; Shao, S.; Hu, Y.; Odman, M. T.; Nenes, A.; Pavur, G. K.; Zou, Y.; Chen, Z.; Smith, R. A.; Burtraw, D.; Driscoll, C. T.: Greater contribution from agricultural sources to future reactive nitrogen deposition in the United States. Earth's Future, doi: 10.1029/2019EF001453, 2020.

Clarisse, L., Clerbaux, C., Dentener, F., Hurtmans, D., and Coheur, P. F.: Global ammonia distribution derived from infrared satellite observations, Nat. Geosci., 2, 479-483, https://doi.org/10.1038/ngeo551, 2009.

Clarisse, L., Shephard, M. W., Dentener, F., Hurtmans, D., Cady-Pereira, K., Karagulian, F., Van Damme, M., Clerbaux, C., and Coheur, P.-F. Satellite monitoring of ammonia: A case study of the San Joaquin Valley, J. Geophys. Res., 115, D13302, https://doi.org/10.1029/2009JD013291, 2010.

Clarisse, L., Van Damme, M., Clerbaux, C., and Coheur, P.-F.: Tracking down global NH_3 point sources with wind-adjusted superresolution, Atmos. Meas. Tech., 12, 5457–5473, https://doi.org/10.5194/amt-12-5457-2019, 2019.

Cooper, M., Martin, R. V., Padmanabhan, A., and Henze, D. K.: Comparing mass balance and adjoint methods for inverse modeling of nitrogen dioxide columns for global nitrogen oxide emissions, J. Geophys. Res. Atmos., 122, 4718-4734, https://doi.org/10.1002/2016jd025985, 2017.

Cooter, E. J., Bash, J. O., Benson, V., and Ran, L.: Linking agricultural crop management and air quality models for regional to national-scale nitrogen assessments, Biogeosciences, 9, 4023-4035, https://doi.org/10.5194/bg-9-4023-2012, 2012.

Dammers, E., Palm, M., Van Damme, M., Vigouroux, C., Smale, D., Conway, S., Toon, G. C., Jones, N., Nussbaumer, E., Warneke, T., Petri, C., Clarisse, L., Clerbaux, C., Hermans, C., Lutsch, E., Strong, K., Hannigan, J. W., Nakajima, H., Morino, I., Herrera, B., Stremme, W., Grutter, M., Schaap, M., Kruit, R. J. W., Notholt, J., Coheur, P. F., and Erisman, J. W.: An evaluation of IASI-NH_3 with ground-based Fourier transform infrared spectroscopy measurements, Atmos. Chem. Phys., 16, 10351-10368, https://doi.org/10.5194/acp-16-10351-2016, 2016.

Dammers, E., Shephard, M. W., Palm, M., Cady-Pereira, K., Capps, S., Lutsch, E., Strong, K., Hannigan, J. W., Ortega, I., Toon, G. C., Stremme, W., Grutter, M., Jones, N., Smale, D., Siemons, J., Hrpcek, K., Tremblay, D., Schaap, M., Notholt, J., and Erisman, J. W.: Validation of the CrIS fast physical NH_3 retrieval with ground-based FTIR, Atmospheric Measurement Techniques, 10, 2645-2667, 10.5194/amt-10-2645-2017, 2017.

Dammers, E., McLinden, C. A., Griffin, D., Shephard, M. W., Van der Graaf, S., Lutsch, E., Schaap, M., Gainairu-Matz, Y., Fioletov, V., Van Damme, M., Whitburn, S., Clarisse, L., Cady-Pereira, K., Clerbaux, C., Coheur, P. F., and Erisman, J. W.: NH_3 emissions from large point sources derived from CrIS and IASI satellite observations, Atmos. Chem. Phys., 19, 12261-12293, https://doi.org/10.5194/acp-19-12261-2019, 2019.

Ellis, R. A., Jacob, D. J., Sulprizio, M. P., Zhang, L., Holmes, C. D., Schichtel, B. A., Blett, T., Porter, E., Pardo, L. H., and Lynch, J. A.: Present and future nitrogen deposition to national parks in the United States: critical load exceedances, Atmos. Chem. Phys., 13, 9083-9095, https://doi.org/10.5194/acp-13-9083-2013, 2013.

Fountoukis, C., and Nenes, A.: ISORROPIA II: a computationally efficient thermodynamic equilibrium model for K^+-Ca^{2+}-Mg^{2+}-NH_4^+-Na^+-SO_4^{2-}-NO_3^--Cl^--H_2O aerosols, Atmos. Chem. Phys., 7, 4639-4659, https://doi.org/10.5194/acp-7-4639-2007, 2007.

Gilliland, A. B., Wyat Appel, K., Pinder, R. W., and Dennis, R. L.: Seasonal NH_3 emissions for the continental united states: Inverse model estimation and evaluation, Atmos. Environ., 40, 4986-4998, https://doi.org/10.1016/j.atmosenv.2005.12.066, 2006.

Hansen, P. C.: The L-curve and its use in the numerical treatment of inverse problems, in: Computational Inverse Problems in Electrocardiology, ed. P. Johnston, Advances in Computational Bioengineering, 119-142, 1999.

Heald, C. L., Collett, J. L., Lee, T., Benedict, K. B., Schwandner, F. M., Li, Y., Clarisse, L., Hurtmans, D. R., Van Damme, M., Clerbaux, C., Coheur, P. F., Philip, S., Martin, R. V., and Pye, H. O. T.: Atmospheric ammonia and particulate inorganic nitrogen over the United States, Atmos. Chem. Phys., 12, 10295-10312, https://doi.org/10.5194/acp-12-10295-2012, 2012.

Henze, D. K., Seinfeld, J. H., and Shindell, D. T.: Inverse modeling and mapping US air quality influences of inorganic PM2.5 precursor emissions using the adjoint of GEOS-Chem, Atmos. Chem. Phys., 9, 5877-5903, https://doi.org/10.5194/acp-9-5877-2009, 2009.

Houlton, B. Z., Boyer, E., Finzi, A. C., Galloway, J., Leach, A., Liptzin, D., Melillo, J., Rosenstock, T. S., Sobota, D., and Townsend, A. R.: Intentional versus unintentional nitrogen use in the United States: trends, efficiency and implications, Biogeochemistry, 114, 11-23, https://doi.org/10.1007/s10533-012-9801-5, 2013.

Kelly, J. T., Baker, K. R., Nowak, J. B., Murphy, J. G., Markovic, M. Z., VandenBoer, T. C., Ellis, R. A., Neuman, J. A., Weber, R. J., Roberts, J. M., Veres, P. R., de Gouw, J. A., Beaver, M. R., Newman, S., and Misenis, C.: Fine-scale simulation of ammonium and nitrate over the South Coast Air Basin and San Joaquin Valley of California during CalNex-2010, J. Geophys. Res. Atmos., 119, 3600-3614, 2014.

Lee, H. M., Paulot, F., Henze, D. K., Travis, K., Jacob, D. J., Pardo, L. H., and Schichtel, B. A.: Sources of nitrogen deposition in Federal Class I areas in the US, Atmos. Chem. Phys., 16, 525-540, https://doi.org/10.5194/acp-16-525-2016, 2016.

Lee, C. J., Martin, R. V., Henze, D. K., Brauer, M., Cohen, A., van Donkelaar, A.: Response of global particulate-matter-related mortality to changes in local precursor emissions. Environ .Sci. Technol., 49, 4335–4344, https://doi.org/10.1021/acs.est.5b00873, 2015.

Li, C., Martin, R. V., Shephard, M. W., Cady-Pereira, K., Cooper, M. J., Kaiser, J., Lee, C. J., Zhang, L., and Henze, D. K.: Assessing the Iterative Finite Difference Mass Balance and 4D-Var Methods to drive ammonia emissions over North America using synthetic observations, J. Geophys. Res. Atmos., 124, 4222-4236, https://doi.org/10.1029/2018jd030183, 2019.

Martin, R. V., Jacob, D. J., Chance, K., Kurosu, T. P., Palmer, P. I., and Evans, M. J.: Global inventory of nitrogen oxide emissions constrained by space-based observations of NO_2 columns, J. Geophys. Res. Atmos., 108, Artn 4537, https://doi.org/10.1029/2003jd003453, 2003.

McQuilling, A. M., and Adams, P. J.: Semi-empirical process-based models for ammonia emissions from beef, swine, and poultry operations in the United States, Atmos. Environ., 120, 127-136, https://doi.org/0.1016/j.atmosenv.2015.08.084, 2015.

NADP (2014). Ambient Ammonia Monitoring Network (AMoN). Wisconsin State Laboratory of Hygiene, 465 Henry Mall, Madison, WI 53706., NADP Program Office. http://nadp.slh.wisc.edu/data/AMoN/ last access: 22 April 2020

NADP (2019). National Atmospheric Deposition Program (NRSP-3). . Wisconsin State Laboratory of Hygiene, 465 Henry Mall, Madison, WI 53706., NADP Program Office. http://nadp.slh.wisc.edu/data/NTN/ last access: 22 April 2020

NOAA (2019). North American Regional Reanalysis. Asheville, NC, National Oceanic and Atmospheric Administration (NOAA). https://www.ncdc.noaa.gov/data-access/model-data/model-datasets/north-american-regional-reanalysis-narr last access: 31 March 2020

NOAA (2020). Meteorological Development Laboratory/Office of Science and Technology/National Weather Service/NOAA/U.S. Department of Commerce: TDL U.S. and Canada Surface Hourly Observations, Research Data Archive at the National Center for Atmospheric Research, Computational and Information Systems Laboratory, https://rda.ucar.edu/datasets/ds472.0/, 1987. last access: 24 Dec 2020.

Pardo, L. H., Robin-Abbott, M. J., Fenn, M. E., Goodale, C. L., Geiser, L. H., Driscoll, C. T., Allen, E. B., Baron, J. S., Bobbink, R., Bowman, W. D., Clark, C. M., Bowman, W. D., Emmett, B., Gilliam, F. S., Greaver, T. L., Hall, S. J., Lilleskov, E. A., Liu, L. L., Lynch, J. A., Nadelhoffer, K. J., Perakis, S. J., Stoddard, J. L., Weathers, K. C., and Dennis, R. L.: Effects and empirical critical loads of nitrogen for ecoregions of the United States, Environ. Pollut. Ser., 25, 129-169, https://doi.org/10.1007/978-94-017-9508-1_5, 2015.

Paulot, F., Jacob, D. J., and Henze, D. K.: Sources and processes contributing to nitrogen deposition: an adjoint model analysis applied to biodiversity hotspots worldwide, Environ. Sci. Technol., 47, 3226-3233, https://doi.org/10.1021/es3027727, 2013.

Paulot, F., Jacob, D. J., Pinder, R. W., Bash, J. O., Travis, K., and Henze, D. K.: Ammonia emissions in the United States, European Union, and China derived by high-resolution inversion of ammonium wet deposition data: Interpretation with a new agricultural emissions inventory (MASAGE_NH3), J. Geophys. Res. Atmos., 119, 4343-4364, https://doi.org/10.1002/2013jd021130, 2014.

Puchalski, M. A., Sather, M. E., Walker, J. T., Lehmann, C. M., Gay, D. A., Mathew, J., and Robarge, W. P.: Passive ammonia monitoring in the United States: comparing three different sampling devices, J. Environ. Monit., 13, 3156-3167, https://doi.org/10.1039/c1em10553a, 2011.

Schiferl, L. D., Heald, C. L., Nowak, J. B., Holloway, J. S., Neuman, J. A., Bahreini, R., Pollack, I. B., Ryerson, T. B., Wiedinmyer, C., and Murphy, J. G.: An investigation of ammonia and inorganic particulate matter in California during the CalNex campaign, J. Geophys. Res. Atmos., 119, 1883-1902, https://doi.org/10.1002/2013jd020765, 2014.

Shen, H., Chen, Y., Hu, Y., Ran, L., Lam, S. K., Pavur, G. K., Zhou, F., and Russell, A. G.~~Armistead, R.~~: Intense Warming Will Significantly Increase Cropland Ammonia Volatilization Threatening Food Security and Ecosystem Health, One Earth, 3, 126-134, https://doi.org/10.1016/j.oneear.2020.06.015, 2020.~~Increased agricultural nitrogen loss via cropland ammonia volatilization under warming, (under review), 2019.~~

Shephard, M. W., Dammers, E., Cady-Pereira, K. E., Kharol, S. K., Thompson, J., Gainariu-Matz, Y., Zhang, J., McLinden, C. A., Kovachik, A., Moran, M., Bittman, S., Sioris, C. E., Griffin, D., Alvarado, M. J., Lonsdale, C., Savic-Jovcic, V., and Zheng, Q.: Ammonia measurements from space with the Cross-track Infrared Sounder: characteristics and applications, Atmos. Chem. Phys., 20, 2277–2302, https://doi.org/10.5194/acp-20-2277-2020, 2020.

Shephard, M. W., and Cady-Pereira, K. E.: Cross-track Infrared Sounder (CrIS) satellite observations of tropospheric ammonia, Atmos. Meas. Tech., 8, 1323-1336, https://doi.org/10.5194/amt-8-1323-2015, 2015.

Shephard, M. W., McLinden, C. A., Cady-Pereira, K. E., Luo, M., Moussa, S. G., Leithead, A., Liggio, J., Staebler, R. M., Akingunola, A., Makar, P., Lehr, P., Zhang, J., Henze, D. K., Millet, D. B., Bash, J. O., Zhu, L., Wells, K. C., Capps, S. L., Chaliyakunnel, S., Gordon, M., Hayden, K., Brook, J. R., Wolde, M., and Li, S. M.: Tropospheric Emission Spectrometer (TES) satellite observations of ammonia, methanol, formic acid, and carbon monoxide over the Canadian oil sands: validation and model evaluation, Atmos. Meas. Tech., 8, 5189-5211, 10.5194/amt-8-5189-2015, 2015.

Stevens, C. J.: Nitrogen in the environment, Science, 363, 578-580, https://doi.org/10.1126/science.aav8215, 2019.

ULB: Ammonia total columns retrieved from IASI measurements from the ANNI-NH_3-v2.2 retrieval algorithm, Universite Libre de Bruxelles (ULB)/Laboratoire atmosphères, milieux et observations spatiales (LATMOS). https://iasi.aeris-data.fr/NH3_IASI_A_data, 2018.

USDA: 2012 Census Ag Atlas Maps - Livestock and Animals, United States Department of Agriculture, National Agricultural Statistics Service, https://www.nass.usda.gov/Publications/AgCensus/2012/Online_Resources/Ag_Atlas_Maps/Livestock_and_Animals, 2012.

USEPA: 2011 National Emissions Inventory Data & Documentation, https://www.epa.gov/air-emissions-inventories/2011-national-emissions-inventory-nei-data, US Environmental Protection Agency Office of Air Quality Planning and Standards, 2015.

USEPA: CMAQ v5.0, US Environmental Protection Agency, http://doi.org/10.5281/zenodo.1079888, 2012.

USEPA: Preparation of Emissions Inventories for the Version 6.1, 2011 Emissions Modeling Platform, US Environmental Protection Agency, https://www.epa.gov/air-emissions-modeling/2011-version-61-technical-support-document, 2014.

USEPA: Air Quality System Data Mart, US Environmental Protection Agency, https://aqs.epa.gov/aqsweb/documents/data_api.html, last access: 06 July 2018.

USGS: Protected Areas Database of the United States (PAD-US) 2.0, U.S. Geological Survey (USGS) Gap Analysis Project (GAP), https://gapanalysis.usgs.gov/padus, 2018.

Van Damme, M., Clarisse, L., Heald, C. L., Hurtmans, D., Ngadi, Y., Clerbaux, C., Dolman, A. J., Erisman, J. W., and Coheur, P. F.: Global distributions, time series and error characterization of atmospheric ammonia (NH_3) from IASI satellite observations, Atmos. Chem. Phys., 14, 2905-2922, https://doi.org/10.5194/acp-14-2905-2014, 2014.

Van Damme, M., Clarisse, L., Dammers, E., Liu, X., Nowak, J. B., Clerbaux, C., Flechard, C. R., Galy-Lacaux, C., Xu, W., Neuman, J. A., Tang, Y. S., Sutton, M. A., Erisman, J. W., and Coheur, P. F.: Towards validation of ammonia (NH_3) measurements from the IASI satellite, Atmos. Meas. Tech., 8, 1575-1591, https://doi.org/10.5194/amt-8-1575-2015, 2015a.

Van Damme, M., Erisman, J. W., Clarisse, L., Dammers, E., Whitburn, S., Clerbaux, C., Dolman, A. J., and Coheur, P. F.: Worldwide spatiotemporal atmospheric ammonia (NH_3) columns variability revealed by satellite, Geophys. Res. Lett., 42, 8660-8668, https://doi.org/10.1002/2015gl065496, 2015b.

Van Damme, M., Whitburn, S., Clarisse, L., Clerbaux, C., Hurtmans, D., and Coheur, P. F.: Version 2 of the IASI NH_3 neural network retrieval algorithm: near-real-time and reanalysed datasets, Atmos. Meas. Tech., 10, 4905-4914, https://doi.org/10.5194/amt-10-4905-2017, 2017.

Van Damme, M., Clarisse, L., Whitburn, S., Hadji-Lazaro, J., Hurtmans, D., Clerbaux, C., and Coheur, P. F.: Industrial and agricultural ammonia point sources exposed, Nature, 564, 99-103, https://doi.org/10.1038/s41586-018-0747-1, 2018.

Walker, J. M., Philip, S., Martin, R. V., and Seinfeld, J. H.: Simulation of nitrate, sulfate, and ammonium aerosols over the United States, Atmos. Chem. Phys., 12, 11213-11227, https://doi.org/10.5194/acp-12-11213-2012, 2012.

Warner, J. X., Wei, Z. G., Strow, L. L., Dickerson, R. R., and Nowak, J. B.: The global tropospheric ammonia distribution as seen in the 13-year AIRS measurement record, Atmos. Chem. Phys., 16, 5467-5479, https://doi.org/10.5194/acp-16-5467-2016, 2016.

Whitburn, S., Van Damme, M., Clarisse, L., Bauduin, S., Heald, C. L., Hadji-Lazaro, J., Hurtmans, D., Zondlo, M. A., Clerbaux, C., and Coheur, P. F.: A flexible and robust neural network IASI-NH_3 retrieval algorithm, J. Geophys. Res. Atmos., 121, 6581-6599, https://doi.org/10.1002/2016jd024828, 2016.

Xu, R. T., Tian, H. Q., Pan, S. F., Prior, S. A., Feng, Y. C., Batchelor, W. D., Chen, J., and Yang, J.: Global ammonia emissions from synthetic nitrogen fertilizer applications in agricultural systems: Empirical and process-based estimates and uncertainty, Glob. Change Biol., 25, 314-326, https://doi.org/10.1111/gcb.14499, 2019.

Yarwood, G., Sunja, R., Mark, Y., and Gary, Z. W.: Updates to the carbon bond chemical mechanism: CB05. Report to the U.S. Environmental Protection Agency., http://www.camx.com/publ/pdfs/cb05_final_report_120805.pdf, 2005.

Zhang, L., Jacob, D. J., Knipping, E. M., Kumar, N., Munger, J. W., Carouge, C. C., van Donkelaar, A., Wang, Y. X., and Chen, D.: Nitrogen deposition to the United States: distribution, sources, and processes, Atmos. Chem. Phys., 12, 4539-4554, https://doi.org/10.5194/acp-12-4539-2012, 2012.

Zhang, L., Chen, Y. F., Zhao, Y. H., Henze, D. K., Zhu, L. Y., Song, Y., Paulot, F., Liu, X. J., Pan, Y. P., Lin, Y., and Huang, B. X.: Agricultural ammonia emissions in China: reconciling bottom-up and top-down estimates, Atmos. Chem. Phys., 18, 339-355, https://doi.org/10.5194/acp-18-339-2018, 2018a.

Zhang, R., Thompson, T. M., Barna, M. G., Hand, J. L., McMurray, J. A., Bell, M. D., Malm, W. C., and Schichtel, B. A.: Source regions contributing to excess reactive nitrogen deposition in the Greater Yellowstone Area (GYA) of the United States, Atmos. Chem. Phys., 18, 12991-13011, https://doi.org/10.5194/acp-18-12991-2018, 2018b.

Zhang, Y. Q., Mathur, R., Bash, J. O., Hogrefe, C., Xing, J., and Roselle, S. J.: Long-term trends in total inorganic nitrogen and sulfur deposition in the US from 1990 to 2010, Atmos. Chem. Phys., 18, 9091-9106, https://doi.org/10.5194/acp-18-9091-2018, 2018c.

Zhao, S., Russell, M. G., Hakami, A., Capps, S. L., Turner, M. D., Henze, D. K., Percell, P. B., Resler, J., Shen, H., Russell, A. G., Nenes, A., Pappin, A. J., Napelenok, S. L., Bash, J. O., Fahey, K. M., Carmichael, G. R., Stanier, C. O., and Chai, T.: A multiphase CMAQ version 5.0 adjoint, Geosci. Model Dev., https://doi.org/10.5194/gmd-2019-287, 2019.

Zhu, C., Byrd, R., Lu, P., and Nocedal, J.: Algorithm 778: L-BFGS-B: Fortran subroutines for large-scale bound-constrained optimization, ACM T. Math. Software, 23(4), 550-560, https://doi.org/10.1145/279232.279236, 1997.

Zhu, L., Henze, D. K., Cady-Pereira, K. E., Shephard, M. W., Luo, M., Pinder, R. W., Bash, J. O., and Jeong, G. R.: Constraining U.S. ammonia emissions using TES remote sensing observations and the GEOS-Chem adjoint model, J. Geophys. Res. Atmos., 118, 3355-3368, https://doi.org/10.1002/jgrd.50166, 2013.

Zhu, L. Y., Henze, D. K., Bash, J. O., Cady-Pereira, K. E., Shephard, M. W., Luo, M., and Capps, S. L.: Sources and impacts of atmospheric NH_3: current understanding and frontiers for modeling, measurements, and remote sensing in North America, Curr. Pollut. Rep., 1, 95-116, https://doi.org/10.1007/s40726-015-0010-4, 2015.

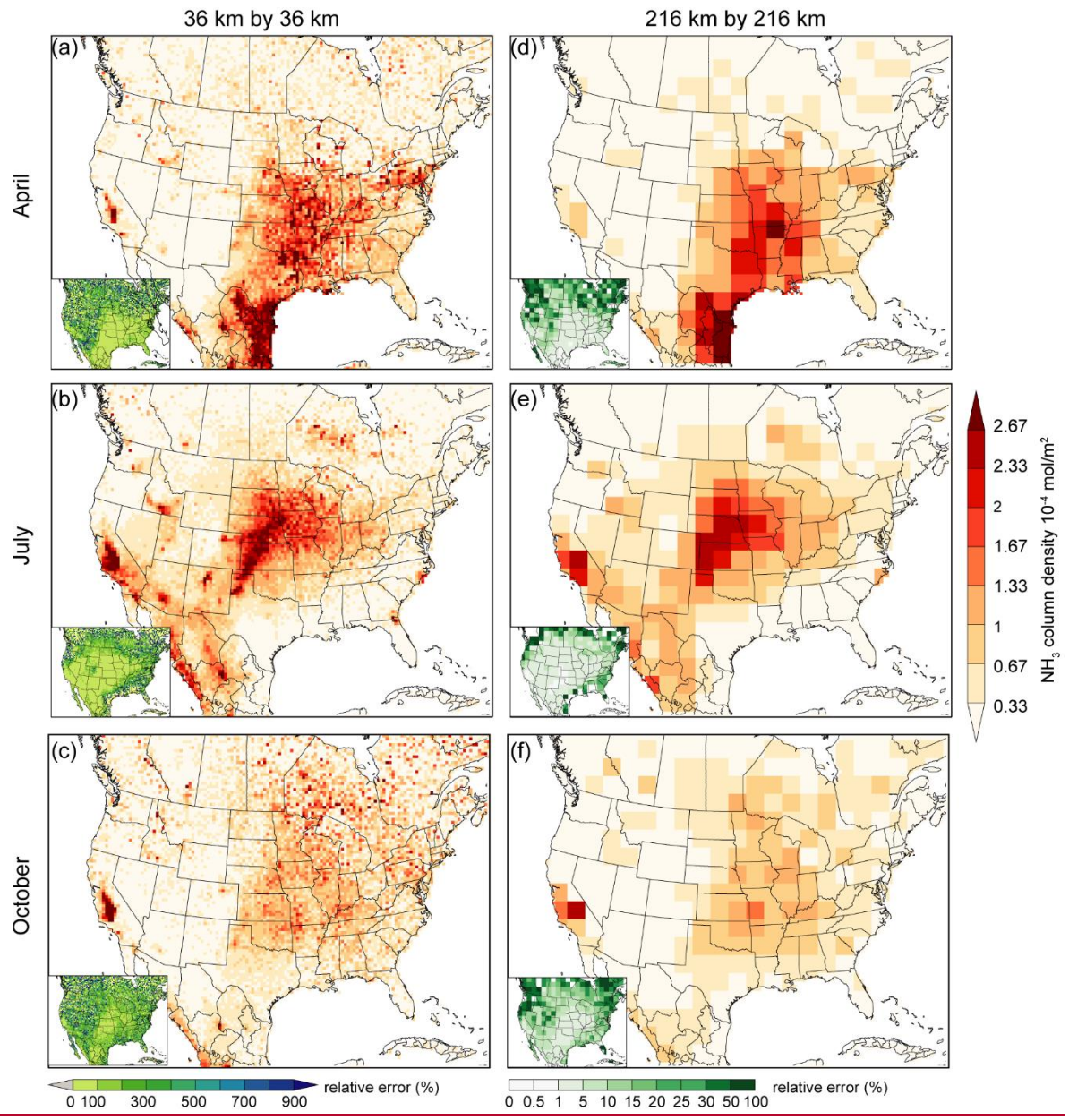

Figure 1 IASI monthly average NH_3 column density in April, July, and October 2011 at 36 km by 36 km (a, b, c) and 216 km by 216 km (d, e, f) resolutions within the model simulation domain of this study. The average relative error associated with the column density is shown in the corner of each plot.

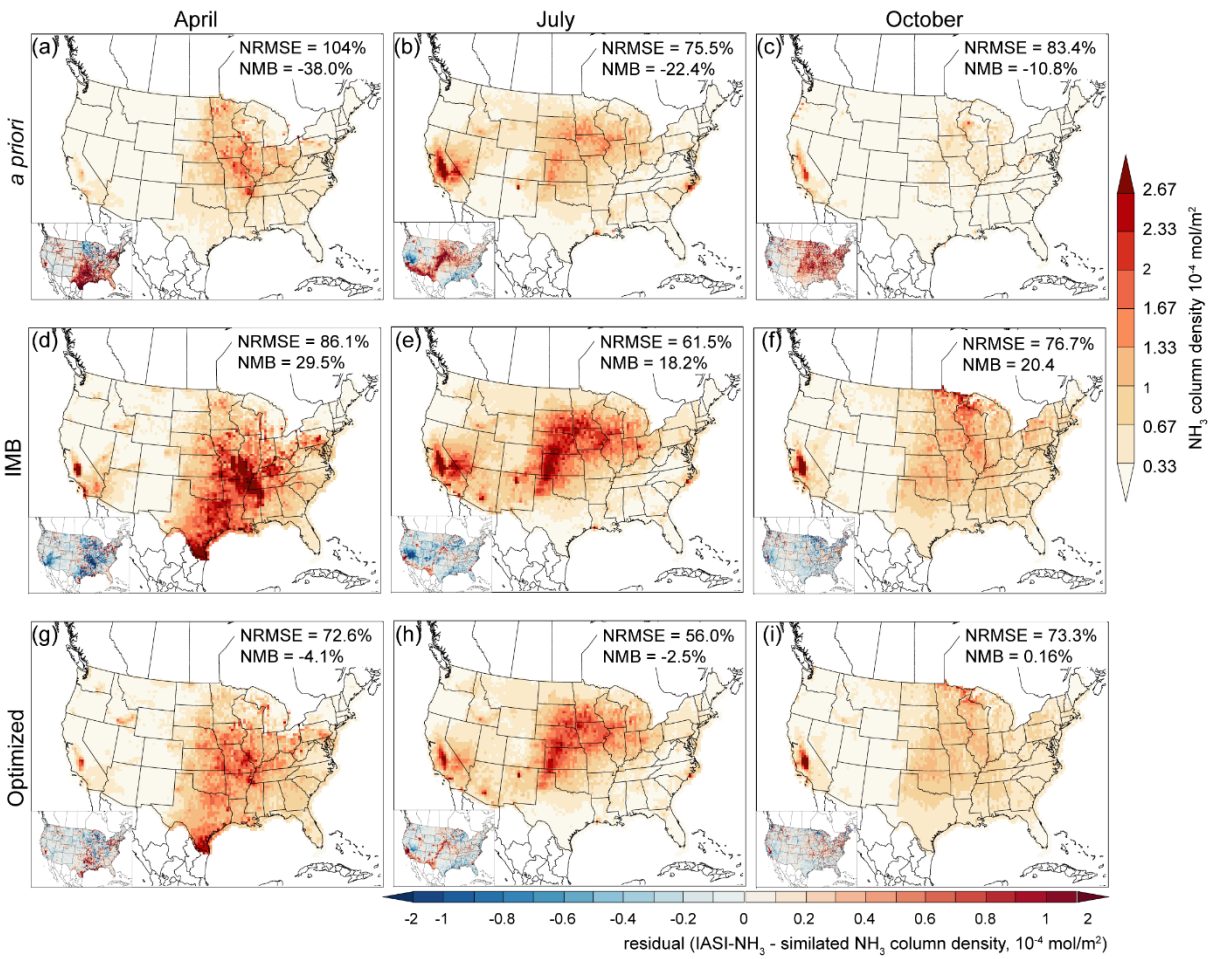

Figure 2 CMAQ simulated monthly average NH_3 column density for April, July, and October 2011 using the *a priori* emissions (a, b, c), the emissions adjusted by IMB (d,e,f), and the final optimized emissions using the hybrid approach (g,h,i). For comparison with the IASI-NH_3 retrievals, simulated NH_3 columns at the passing time were derived when there are observations in that grid cell. Normalized root mean square error (NRMSE) and normalized mean bias (NMB) between the simulated values and IASI-NH_3 are provided. Residue map (IASI-NH_3 – simulated NH_3 column densities) is shown in the corner of each plot.

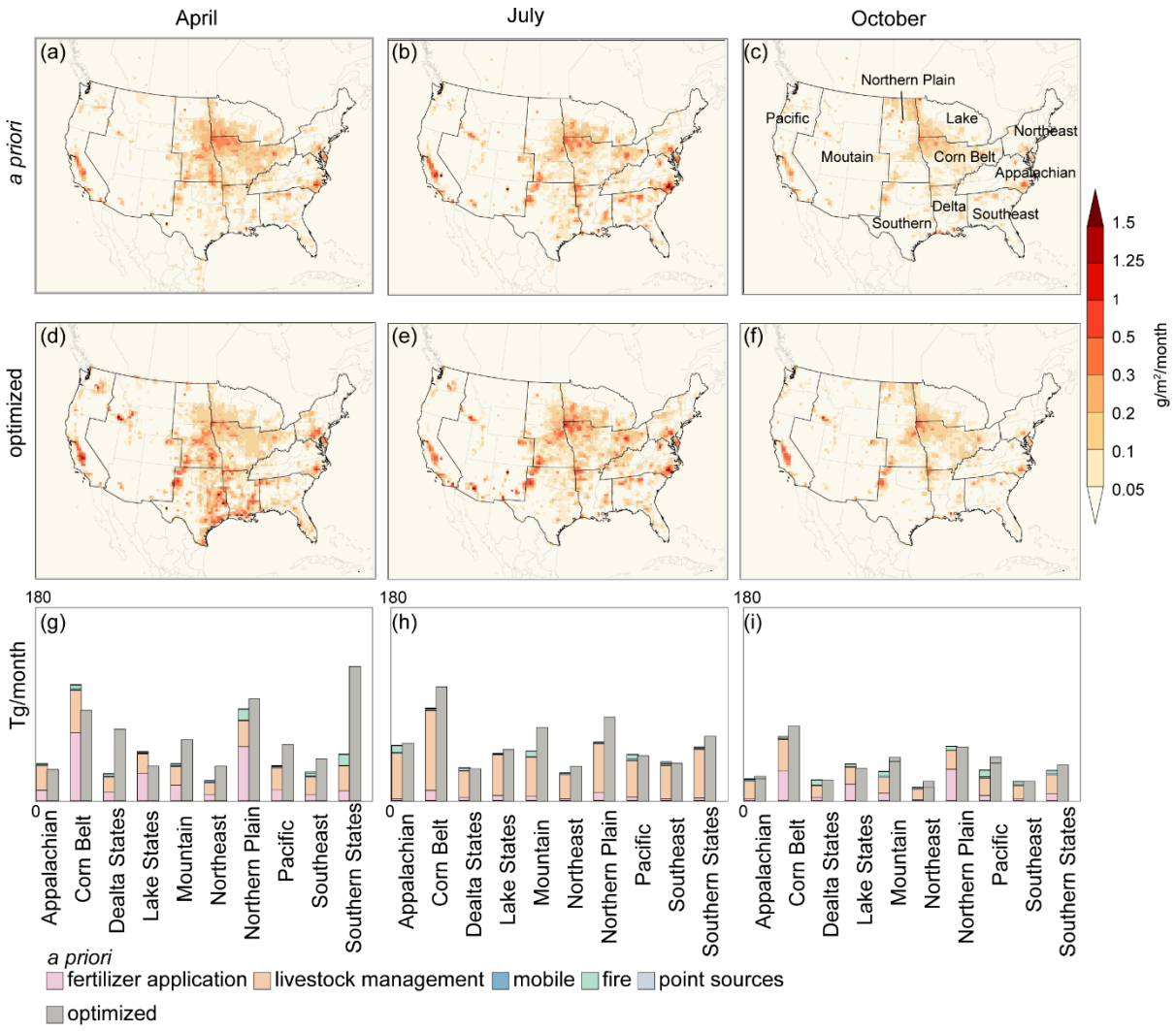

Figure 3 The spatial distribution of monthly total NH_3 emission from the *a priori* (a, b, c) and optimized (d, e, f) estimates in April, July, and October. The total emission based on the *a priori* and optimized estimates are summarized for each USDA Farm Production region (g, h, i). The source contributions to total emission are shown for the *a priori* estimates.

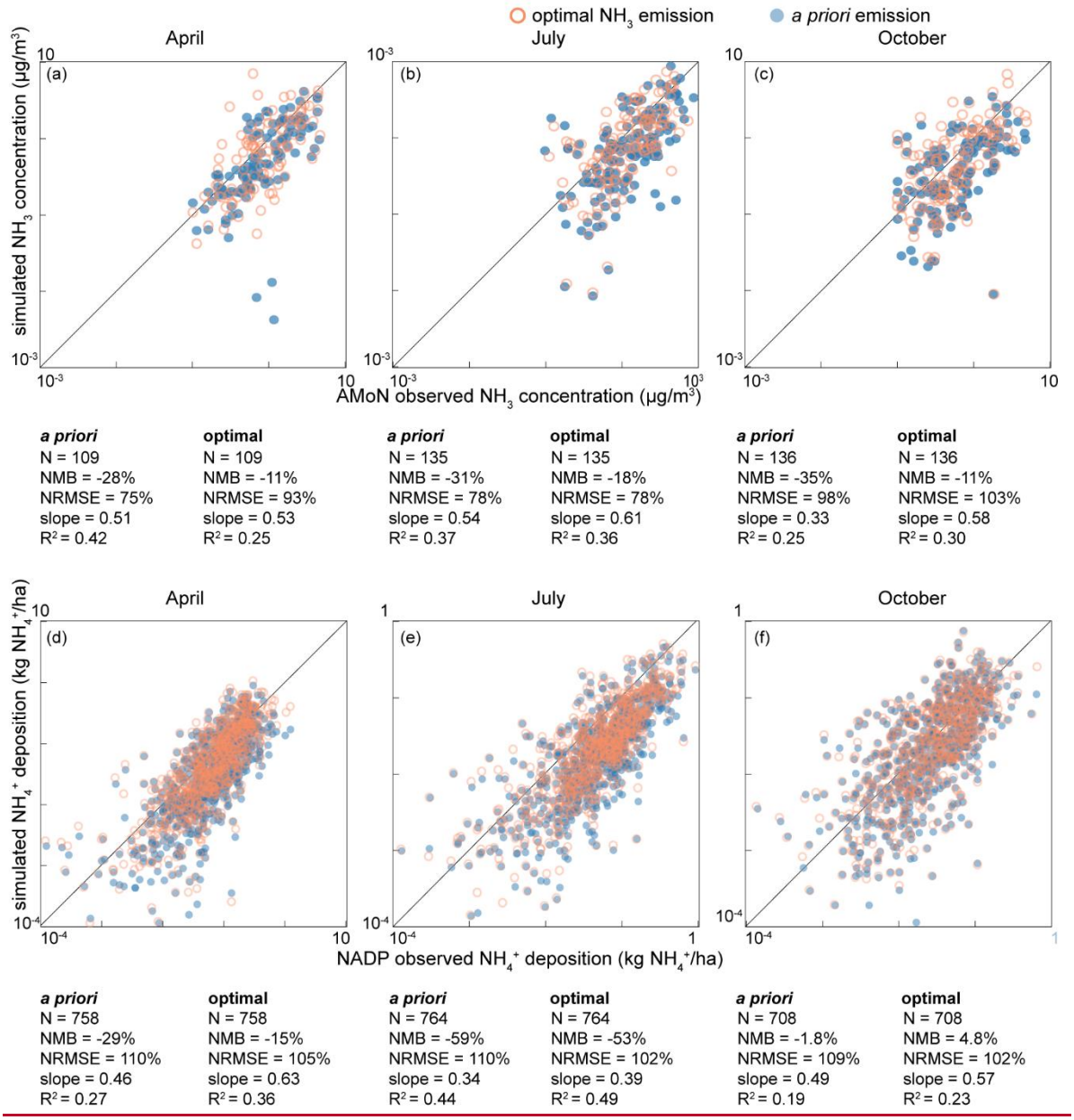

Figure 4 Evaluation of the simulated NH_3 surface concentration (a, b, c) and NH_4^+ wet deposition (d, e, f) against biweekly NH_3 concentration observations from AMoN and weekly NH_4^+ wet deposition observations from NADP, respectively. The orange circles and blue dots represent comparison using the *a priori* and optimized NH_3 emission estimates, respectively. Summary statistics including sample size (N), normalized mean bias (NMB), normalized root mean square error (NRMSE), least square error regression slope and intercept, and R square (R^2) for all comparisons are listed below the plots.

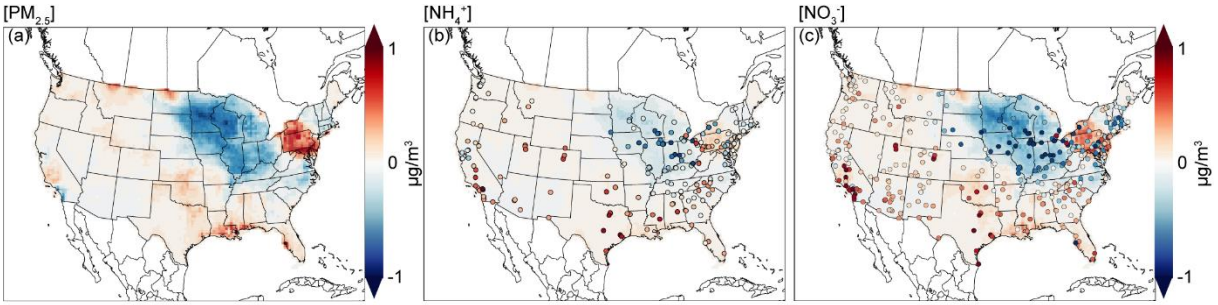

Figure 5 The changes in monthly average $PM_{2.5}$, NH_4^+, and NO_3^- mass concentration in April due to the NH_3 emission adjustment in the optimized estimates. The change is defined as $conc_{optimized} - conc_{a\ priori}$, where $conc_{optimized}$ and $conc_{a\ priori}$ represents the simulated monthly average mass concentration using the optimized and *a priori* NH_3 emission estimates, respectively. The difference between the observed NH_4^+, and NO_3^- mass concentration and simulated concentrations using the *a priori* NH_3 emission ($conc_{obs} - conc_{a\ priori}$, where $conc_{obs}$ represents the observed monthly average mass concentration) are overlaid using colored dots with the same color scheme.

720

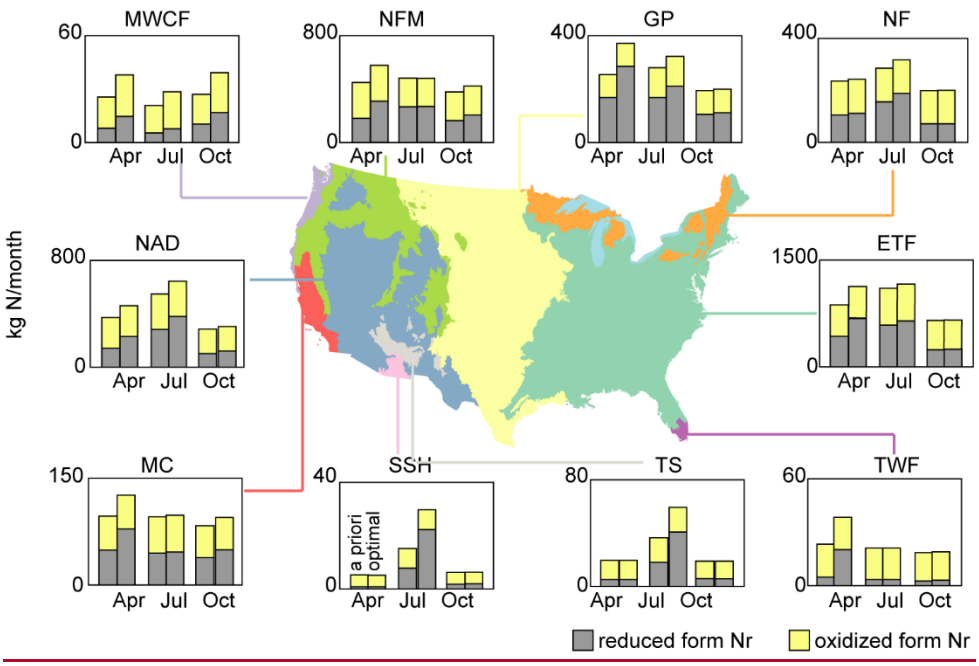

Figure 6 The changes in the simulated monthly reactive nitrogen (Nr) deposition amount in protected areas for biodiversity conservation caused by the emission adjustment in April, July, and October. For each month, the left bar is for the *a priori* deposition amounts and the right bar is for the optimized deposition amounts. The deposition is grouped for 10 level I ecoregions defined by the Commission for Environmental Cooperation, including Northern Forests (NF), Great Plains (GP), Northwestern Forested Mountains (NFM), Marine West Coast Forest (MWCF), North American Deserts (NAD), Mediterranean California (MC), Southern Semiarid Highlands (SSH), Temperate Sierras (TS), and Tropical Wet Forests (TWF).

Table 1 Statistical summary of the correlation between simulated monthly average NH_4^+ and NO_3^- concentrations and observations in April[a]

NH_4^+	Midwest		Penn		Other	
	a priori	optimized	*a priori*	optimized	*a priori*	optimized
N	47		37		115	
NMB	0.18	0.03	0.03	0.33	-0.24	-0.2
NRMSE	0.39	0.29	0.33	0.59	0.45	0.49
slope	0.52	0.60	0.47	0.33	0.74	0.28
R^2	0.60	0.65	0.34	0.49	0.22	0.08
NO_3^-	Midwest		Penn		Other	
	a priori	optimized	*a priori*	optimized	*a priori*	optimized
N	69		38		240	
NMB	0.50	0.22	0.10	0.58	-0.66	-0.69
NRMSE	0.75	0.51	0.27	0.72	0.82	1.03
slope	0.44	0.50	0.18	0.48	0.33	0.48
R^2	0.76	0.72	0.31	0.67	0.13	0.67

[a] The correlation between observed concentrations and simulated ones based on *a priori* and optimized NH_3 emission estimates are compared. The sites are grouped as the Midwest region, Pennsylvania state and surrounding areas, and other areas.

NH_4^+	Midwest		Penn		Other	
	a priori	optimized	*a priori*	optimized	*a priori*	optimized
N	47		37		115	
NMB	0.27	0.22	0.00	0.07	-0.35	-0.35
NRMSE	0.40	0.35	0.28	0.30	0.45	0.44
slope	0.52	0.54	0.41	0.39	0.60	0.65
R^2	0.57	0.65	0.24	0.18	0.25	0.28
NO_3^-	Midwest		Penn		Other	
	a priori	optimized	*a priori*	optimized	*a priori*	optimized
N	69		38		240	
NMB	0.64	0.55	0.25	0.43	-0.39	-0.38
NRMSE	0.96	0.88	0.66	0.73	0.63	0.65
slope	0.44	0.46	0.29	0.29	0.62	0.55
R^2	0.76	0.78	0.33	0.31	0.28	0.25

[a] The correlation between observed concentrations and simulated ones based on *a priori* and optimized NH_3 emission estimates are compared. The sites are grouped as the Midwest region, Pennsylvania state and surrounding areas, and other areas.

725